University of Reading

3 µm water vapor self- and foreign-continuum: new method for determination and new insights into the self-continuum

Article

Accepted Version

Creative Commons: Attribution-Noncommercial-No Derivative Works 4.0

Birk, M., Wagner, G., Loos, J. and Shine, K. P. ORCID: https://orcid.org/0000-0003-2672-9978 (2020) 3 µm water vapor self- and foreign-continuum: new method for determination and new insights into the self-continuum. Journal of Quantitative Spectroscopy and Radiative Transfer, 253. 107134. ISSN 0022-4073 doi: https://doi.org/10.1016/j.jqsrt.2020.107134 Available at https://centaur.reading.ac.uk/91123/

It is advisable to refer to the publisher's version if you intend to cite from the work. See Guidance on citing.
Published version at: http://dx.doi.org/10.1016/j.jqsrt.2020.107134
To link to this article DOI: http://dx.doi.org/10.1016/j.jqsrt.2020.107134

Publisher: Elsevier

All outputs in CentAUR are protected by Intellectual Property Rights law, including copyright law. Copyright and IPR is retained by the creators or other copyright holders. Terms and conditions for use of this material are defined in the End User Agreement.

www.reading.ac.uk/centaur

University of Reading

CentAUR

Central Archive at the University of Reading

Reading's research outputs online

3 µm water vapor self- and foreign-continuum: New method for determination and new insights into the self-continuum

M. Birk[a*], G. Wagner[a], J. Loos[a], K.P. Shine[b]

[a]Remote Sensing Technology Institute, German Aerospace Center (DLR), D-82234 Wessling, Germany

[b]Department of Meteorology, University of Reading, Earley Gate, Reading RG6 6BB, UK

*Corresponding author: Manfred Birk, manfred.birk@dlr.de, +498153283084

Email addresses of all authors

manfred.birk@dlr.de

georg.wagner@dlr.de

joep.loos@web.de

k.p.shine@reading.ac.uk, Orcid ID 0000-0003-2672-9978

Abstract

The H_2O self- and foreign- in-band continua in the region 3400-3900 cm^{-1} were experimentally determined for 296 and 353 K from multispectrum fitting results of line parameters using the Hartmann-Tran line profile (HTP) and Rosenkranz line mixing. The continua were extracted from the baselines which were determined in the microwindow-based multispectrum fits. Continua were then obtained by simultaneous fitting of all baselines from measurements containing continuum information. The self-continuum at 296 K was determined from self-broadened measurements and agrees with that determined from air broadened measurements. The overall shape and strength of the new self-continuum agrees with the CAVIAR results between 3600 and 3800 cm^{-1} but differences exceed the stated uncertainties at higher and lower wavenumbers. Moreover, the new self-continuum is much smoother, has no gaps and is obtained with a high resolution of 2.4 cm^{-1}. The self-continuum was fitted as sum of modeled bound and quasi-bound dimer spectra. From rotational constants, the bound dimer parallel and perpendicular band shapes of the near prolate symmetric top molecule were calculated and used as kernels to fit fundamental wavenumbers, relative band intensities and partitioning of parallel and perpendicular band type, while the integral of the band intensities of the four fundamentals was fixed to published experimental/theoretical data. A dimerization constant for the bound dimer of K_{Db}=0.026(2) atm^{-1} and the quasi-bound dimer of K_{Dq}=0.044(5) atm^{-1} was derived from the fits.

The foreign-continuum has no gaps, a spectral resolution of 6-16 cm^{-1}, and is about 40% smaller than the MT_CKD3.2 continuum model. It has a distinctly different shape showing a pronounced P-Q-R branch structure. The foreign-continuum shape is narrower than the monomer band shape which is also true for the MT_CKD3.2 continuum model. The CAVIAR foreign-continuum is much noisier but on average is in good agreement with the new measurements.

Keywords

Water vapor, self-continuum, foreign-continuum, Fourier Transform spectroscopy, water dimer

1. Introduction

The water vapor continuum is absorption found in pure water vapor and water/air spectra which cannot be attributed to Voigt based rotational or rovibrational water lines. There are two distinct contributions, the self-continuum (SC) and the foreign-continuum (FC). While the SC optical depth is proportional to the water pressure squared, the FC optical depth is proportional to the water pressure and the air (or other broadening gas) pressure. The history of the continua is summarized for example in [Shine2012]. The name continuum is related to the absence of high resolution features. It is rather weak when compared to the typical rotational and rovibrational water vapor bands. In the following the MT_CKD continuum will be introduced, the relevance of the continuum for climate and remote sensing discussed, and the common method for extraction of the continuum briefly mentioned. While these subsections are more general, the subsection about the experimental continuum data is focused on the near infrared region close to the spectral range around 3 µm relevant to this work. In the final subsection the current understanding of the physical background of the continuum is discussed.

1.1 MT_CKD Continuum Model

A commonly used parameterization of the continuum is the MT_CKD (Mlawer-Tobin_Clough-Kneizys-Davies) continuum model [Mlawer2012]. The first versions of its predecessor, the CKD continuum model [Clough1989], are based on older laboratory measurements mostly by Burch and co-workers [Burch1982;Burch1984] in the 1980s in the range 330-2000 cm^{-1} (for details see [Clough1989]). The CKD continuum model is constructed from uniformly modified Lorentzian profiles of the water lines listed in the HITRAN database to fit the experimental continuum. Although the spectral range of the above mentioned laboratory measurements is limited, the total range from 0 to 20000 cm^{-1} given by CKD model is based on this line profile modification applied at all wavenumbers. For the FC and SC separately, there is one line-profile function which is multiplied with the Voigt function of each line and contains a super-Lorentzian and sub-Lorentzian region. The local lines in a ±25 cm^{-1} interval are omitted, except for a so-called plinth/pedestal, which is the value of the Lorentz-line at ±25 cm^{-1} which is subtracted from the line

contribution within 25 cm^{-1} of line centre and added to the continuum. Contributions from all lines are summed. Based on remote sensing results, the CKD continuum model was updated several times and finally replaced by the MT_CKD formalism since the many changes could not be well represented by the CKD formalism [Mlawer2012]. The MT_CKD continuum model is composed of two parts, an allowed term and a so-called 'weak interaction' term. The allowed term covers the sub-Lorentzian part only while the weak interaction term gives most of the in-band and, especially in case of the SC, also part of the in-between band continuum. While the FC is treated as temperature independent, the rather strong temperature dependence of the SC is extrapolated from experimental data in the range 296-338 K to lower temperatures.

The tabulated MT_CKD SC model values are larger than the FC values. The maximum in-band SC values for the ν_2 band around 1600 cm^{-1} and the ν_1/ν_3 bands around 3800 cm^{-1} are 5-6x10^{-21} $cm^2molecule^{-1}atm^{-1}$, while the FC is about 11 times weaker. In between the bands there is still a significant SC while the FC is very small. The in-between band values of the SC decrease with increasing wavenumber, for 1140 cm^{-1} they are 1.2x10^{-22} $cm^2molecule^{-1}atm^{-1}$ (46 times smaller than the in-band value), decrease by a factor of 15 at 2600 cm^{-1} and by a factor of 24 at 4770 cm^{-1}. The FC values in-between bands are below 6x10^{-26} $cm^2molecule^{-1}atm^{-1}$ and, thus, much smaller when compared to the SC for the in-between band position. All values were taken from MT_CKD3.2 [Mlawer2019].

1.2 Relevance of continuum for climate and remote sensing

For atmospheric conditions for the case of the in-band continua for 1 atm total pressure (boundary layer conditions) and 20 mbar H_2O, the FC optical depth is about 4 times larger than that of the SC. In contrast, the impact of the FC in the atmospheric window region 800-1200 cm^{-1} is small, while that of the SC is significant for tropical conditions but negligible under subarctic winter conditions.

The climate impact of the continuum is twofold. While below 2000 cm^{-1} the OLR (outgoing longwave radiation) is of importance, in the range 2000-10000 cm^{-1} the absorption of solar radiation is relevant. According to [Paynter2011] the OLR decrease due to the SC and FC for tropical condition is 8.4 and 2.7 W/m^2, respectively. The solar radiation reaching the Earth's surface (in cloud-free skies), globally averaged, is reduced by about 1.2 W/m^2 for the MT_CKD2.5 continuum model and 0.74 W/m^2 more for the CAVIAR (Continuum Absorption in the Visible and Infrared and its Atmospheric Relevance) continuum [Ptashnik2012]. These contribute a few % of components of the Earth's radiation balance.

The FC in the region 1300-2000 cm^{-1} is important since the region is used to derive water profiles from nadir viewing satellite instruments utilized in numerical weather predictions [Newman2012]. Certainly, the water continuum, and its role changing atmospheric transmittance or radiance, is of potential importance for many remote sensing applications, both in-band and between-band, including determination of cloud properties [Shine2012].

1.3 Determination of continuum in the past

The continuum is usually obtained from transmittance spectra (absorption coefficient spectra in the case of CRDS (cavity ring down spectroscopy) measurements) by removing local line contributions calculated typically from HITRAN line parameters (using the Voigt line shape). To avoid line parameter induced errors only microwindows (troughs) between lines are used. This leads to large gaps in the derived continuum in regions with many lines. Thus, this method unfortunately yields a relatively coarse resolution, in particular for the in-band FC which is more susceptible to local line errors since at 1 bar the water lines are 10 times wider than pure water lines at 20 mbar. A broadband determination of the FC with low total pressure measurements gives a too weak continuum to be measured with usual configurations of spectrometers like FTS (Fourier-Transform spectrometer).

1.4 Previous measurements of H_2O near-IR continua

Historically, many measurements of the SC and FC in the thermal infrared and microwave are available [Mlawer2012,Mlawer2019,Shine2012,Shine2016]. Adjustments to these continua are still necessary [Cormier 2005,Mlawer 2019], but it is generally quite well-characterized. This is not the case in the near-IR (NIR), which is the focus here.

In-band continua from laboratory measurements have been reported for both the SC and FC, for various NIR bands [Burch1985,Paynter2009,Ptashnik2004,Ptashnik2019]. These studies are in reasonable agreement, but the dense line structure means that the continuum can only be obtained at certain wavenumbers, and uncertainty in spectral line parameters is the dominant source of uncertainty [Ptashnik 2019]. Nevertheless, these works indicate significant broad but distinct spectral features, attributed to the water dimer, that are not represented in MT_CKD.

The between-band situation in the NIR is less clear. Most SC measurements are available in the 2500 cm^{-1} between-band region [Shine2016,Richard2017]; at room temperature there is an order of magnitude spread in the SC strength and disagreement in the temperature dependence. Many fewer measurements

are available at wavenumbers greater than 4000 cm^{-1}; most reported SC and FC measurements are from two laboratories using FTS (including those associated with the CAVIAR (Continuum Absorption in the Visible and Infrared and its Atmospheric Relevance) project and Tomsk (who also report a measurement using the photo-acoustic method [Kapitanov2018]) and one laboratory (Grenoble) using CRDS and related cavity-laser techniques. Much of this work was reviewed in [Shine2016], with more recent measurements reported by [Campargue2016,Richard2017,Lechevallier2018,Vasilchenko2019]. A general problem with FTS measurements is the low sensitivity. In case of the weak in-between band signals the stability of the instrument baseline becomes a severe source of uncertainty. For a given absorption path, the intensity is limited by the vapor pressure which decreases with temperature. Lower temperatures, significant for the atmosphere, can thus not be covered. Many of the cavity measurements have been made near room temperature, with selected ones at higher temperature. There is currently a dearth of measurements at lower temperatures. For the SC, the consistency between measurements and MT_CKD varies with both temperature and wavenumber. In the 2.1 µm window the high-temperature FTS measurements appear consistent the cavity-laser measurements, assuming a dimer-like temperature dependence. This is not the case in the 1.6 µm window, with the cavity-laser measurements indicating a smaller temperature dependence. One important possibility [Shine2016] is that the SC changes shape with temperature, and thus there is no common temperature dependence for the SC at all between-band wavenumbers, which is contrary to the representation in MT_CKD.

For the between-band FC, there is only one set of FTS measurements covering a significant wavenumber range [Ptashnik2012] and a more limited set of cavity-laser measurements at selected wavenumbers [Mondelain2015,Vasilchenko2019,Mondelain2020]. Although these measurements are not in full agreement, they consistently indicate that the FC in the center of the windows is significantly higher than MT_CKD. The derivation of FC from laboratory measurements is reliant on an accurate SC, but on the other hand, the weaker temperature dependence means that observations at elevated temperatures are likely more relevant to atmospheric conditions. Although no temperature dependence could be detected within the measurement uncertainties in [Ptashnik2012] this does not rule out the possibility of a weak dependence, as has been suggested in other spectral regions [Cormier2005].

1.5 Physical background of continuum

About half of the 3 µm in-band SC at room temperature (somewhat less for the 6 µm band) consists of the spectrum of the bound H_2O dimer [Epifanov1997;Ptashnik2011; Serov2017;Ptashnik2019]. A second component is the quasi-bound (metastable) dimer showing the spectrum of the extremely broadened water monomer. Serov postulated a third term caused by middle wing deviations from the Voigt line profile. This was necessary since the amount of stable and metastable dimers calculated from virial coefficients represented by the total dimerization equilibrium constant K_{eq} was too small to model the observed continuum. [Ptashnik2011;Ptashnik2019] tried to model the continuum without middle wing contributions but also found disagreement with the equilibrium constant. The bound dimer spectrum shows discrete bands differing from the monomer bands (see Figure 5 in [Ptashnik2011], Figure 5 in [Ptashnik2019]). The different contributions to the SC together with the different bound dimer bands cause a strong spectral dependence of the temperature dependence of the continuum. The amount of bound dimer is significantly reduced with increased temperature due to dissociation. A spectrum of the bound dimer can also be seen in the SC below 50 cm^{-1} [Odintsova2019]. Rotationally resolved structure of dimer lines in gaseous water was found by [Serov2014] between 188 and 258 GHz. Ma et al. give theoretical calculations of the SC and its temperature dependence using far wing impact theory alone [Tipping1995,Ma2008]. Although the far wings cannot explain the entire SC because of the statements above, a contribution of this type is still possible.

It should be mentioned that spectroscopic measurements of H_2O samples at atmospheric conditions are not the favorite method to determine H_2O dimer spectroscopy, since only about 0.1% of the water at 20 mbar is bound dimer at 296K, as can be calculated from the dimerization equilibrium constant. [Serov2017]. There is rather long history of spectroscopic investigations of the H_2O dimer in molecular beams and matrix isolation spectroscopy, listed in review [Mukhopadhyay2015].

In contrast to the SC, the FC does not show strong in-between band contributions and is mostly interpreted as far wing deviation from the Lorentz profile. A theoretical model is based on the impact theory developed by Tipping and Ma [Tipping1995] covering SC and FC. Insights into far wings are available from measurements and analysis of Ar-broadened HCl [Tran2017], which is a simple diatomic molecules with lower line density than H_2O, thus line wings are visible farther away from the line center. Super- and sub-Lorentzian contributions were modeled applying Classical Molecular Dynamics Simulations (CMDS). While close to the band center super Lorentzian lineshape dominates, the high *J* lines showed sub-Lorentzian behavior, which was attributed to line mixing.

2. Continuum determination

2.1 Method

Water measurements between 1800 and 4000 cm^{-1} with high quality line parameters already determined [Loos2017;Loos2017a] allowed the prototyping of a new method for continuum determination which is described here. The major advantage of the method is the use of the same spectra to derive the spectroscopic line parameter database and the continuum information. Thus, the occurrence of large spectral gaps and systematic errors due to local line errors present in previous work can be avoided. This is especially an improvement for the in-band determination of the FC where a high line density of local water lines is present.

The spectra are fitted within short microwindows with a multispectrum fitting approach utilizing the Hartmann-Tran line profile [Tran2013;Tran2014] including Rosenkranz line mixing. Since also instrument properties like the instrumental line shape were well characterized, the spectra could be fitted down to the noise level. Since the input to the line fitting are transmittance spectra (which were obtained by dividing sample spectra by empty cell spectra), the fitted baseline contains the continuum information. The continuum is then retrieved from the baselines. It should be emphasized that systematic errors would occur when only using the Voigt profile for analyzing the spectra since a) it would not be possible to fit the spectra down to the noise level, which in turn would cause systematic errors in the fitted baseline, and b) an effective Voigt fit of non-opaque laboratory spectra leads to systematically too small Lorentz broadening parameters [Birk2016] due to speed dependence and Dicke narrowing which would also introduce systematic errors in the fitted baselines. Furthermore, it should be mentioned that line mixing influences the entire Lorentz profile including regions far away from the line center. Due to the multispectrum approach utilizing both, opaque and non-opaque, spectra combined with the Hartmann-Tran line profile and Rosenkranz line mixing lines with opaque centers can also be fitted and, thus, a reliable baseline is available even in this case.

It should be noted that the measurements were primarily made to determine line parameters and not the continuum. So neither the measurement plan nor the baseline stability was adapted to optimum continuum determination. To use the fitted baselines to determine the continuum is only a step in developing the simultaneous multispectrum fitting of continuum and line parameters. The results are useful for the in-band region but not for the in-between bands regions.

2.2 Data

In the previously mentioned publications of Loos et al. the details on the measurements and instrumental setup are given. 15 pure water measurements and 24 air broadened measurements at 296 K, as well as 15 air broadened measurements at low or elevated temperature, 5 at 213 and 253 K and 10 at about 350 K, were recorded. The fitting was achieved in three steps: multispectrum fitting of the pure water measurements was carried out first, then of the air broadened data and then of the data at low and high temperatures. In each step, line parameters were determined and then kept fixed in the next steps. For example, line positions and intensities as well as self broadening line profiles were fitted in the first step and kept fixed in the following steps. In the case of pure water measurements, the spectrum was cut in 0.25 cm^{-1} to 0.75 cm^{-1} sized microwindows and 0.5 cm^{-1} to 3 cm^{-1} in case of foreign broadening. The line profiles were cut at ±100 cm^{-1} from their centers. Thus, all lines were considered which are inside a distance of ±100 cm^{-1} from the microwindow boundaries. The final multispectrum fitting is carried out with all line parameters in the final state to correctly account for the influence of the updated lines in the ±100 cm^{-1} range. This guarantees that there is no local line influence on the baseline and hence not on the continuum. A baseline quadratic in wavenumber is fitted for each microwindow and each spectrum.

Initially, we tried to use the fitted baseline data to retrieve the continua. Unfortunately, it turned out that there were some problems: a) In the case of self-broadened measurements there was line mixing present which initially was rarely fitted, b) In some cases opaque regions covered most or all of a microwindow and no baseline was available due to the small microwindow width.

Because of this, new microwindows were defined with substantially larger width ranging from 6 to 16 cm^{-1}. Microwindow boundaries were placed at points with minimum absorption. Larger microwindows required to fit or refit line mixing in order to get residuals close to the noise level. Reaching the noise level proves that the continuum does not have higher resolution than the microwindow widths. Since a large microwindow covers several narrow microwindows of the original fit there are fewer baseline parameters in the new fit than in the old fit. More baseline parameters defining smaller wavenumber segments allow the incorporation of line profile information. The narrow quadratic polynomial baseline segments can approximate line mixing while the wide baseline polynomials cannot. The width of the line mixing contribution is too small for the wide baseline polynomials. If not considered, line mixing can fake a high resolution continuum. Figure 1 shows the impact of the line mixing on the spectrum of concatenated baselines of one of the measurements (case #4 in Table 1). The improvement of the baseline quality and thus the derived continuum is considerable. The reason for the high importance of

self line mixing is the about 6 times larger self line mixing parameter when compared to air line mixing.

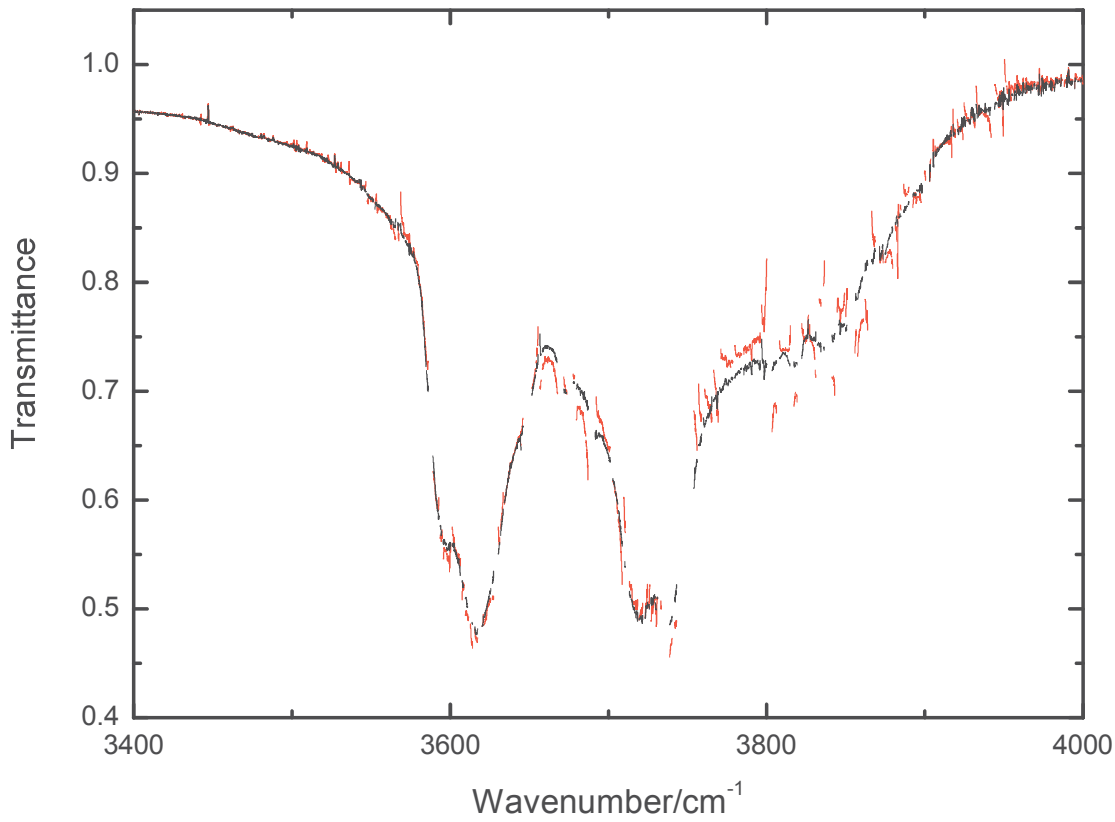

Figure 1. Concatenated fitted baselines from measurement #4, Table 1. Red: no line mixing or line mixing from narrow microwindows, black: with line mixing from wide microwindows.

When line mixing was (re)fitted for a specific line, the Lorentzian width and the pressure induced line shift were also refitted. Surprisingly, the air-broadened measurements did not require refitting the line mixing already covered by [Loos2017,Loos2017a], who fitted more air line mixing parameters than self line mixing parameters. Together with the initially somewhat wider microwindows for air-broadened measurements this may be the reason that there was not so much line mixing hidden in the baseline parameters. In the case of the self-broadened measurements line mixing had not been fitted in the

previous analysis. As stated above this can be attributed to the narrow microwindows which easily hide the line mixing effects in the quadratic baseline polynomial. The self broadening analysis applied narrower microwindows than the air broadening analysis due to the smaller pressure-broadened widths. The above mentioned microwindow boundary selection has the further advantage that baseline information is available close to both boundaries which enables interpolation of the baseline. For the air-broadened measurements, in several microwindows the central region was opaque and so did not have enough information to fit a quadratic baseline polynomial. Thus, the polynomial degree was limited to 1, which was applied to all microwindows. This was justified by verifying that the residuals of the multispectrum fit were still within the noise level. For the self-broadened measurements, the quadratic baseline was maintained. Figures 2 and 3 show examples of the multispectrum fit of pure H_2O and air-broadened measurements at room temperature. The measured spectra, the calculated spectra obtained from the fitted parameters (including baseline), and the residuals for the individual measurements can be seen. It can be seen that residuals are mostly within the noise level. After updating the spectroscopic database for the self-broadened line shape, the spectra were refitted with the narrow microwindows to ensure sufficient spectral resolution for the SC.

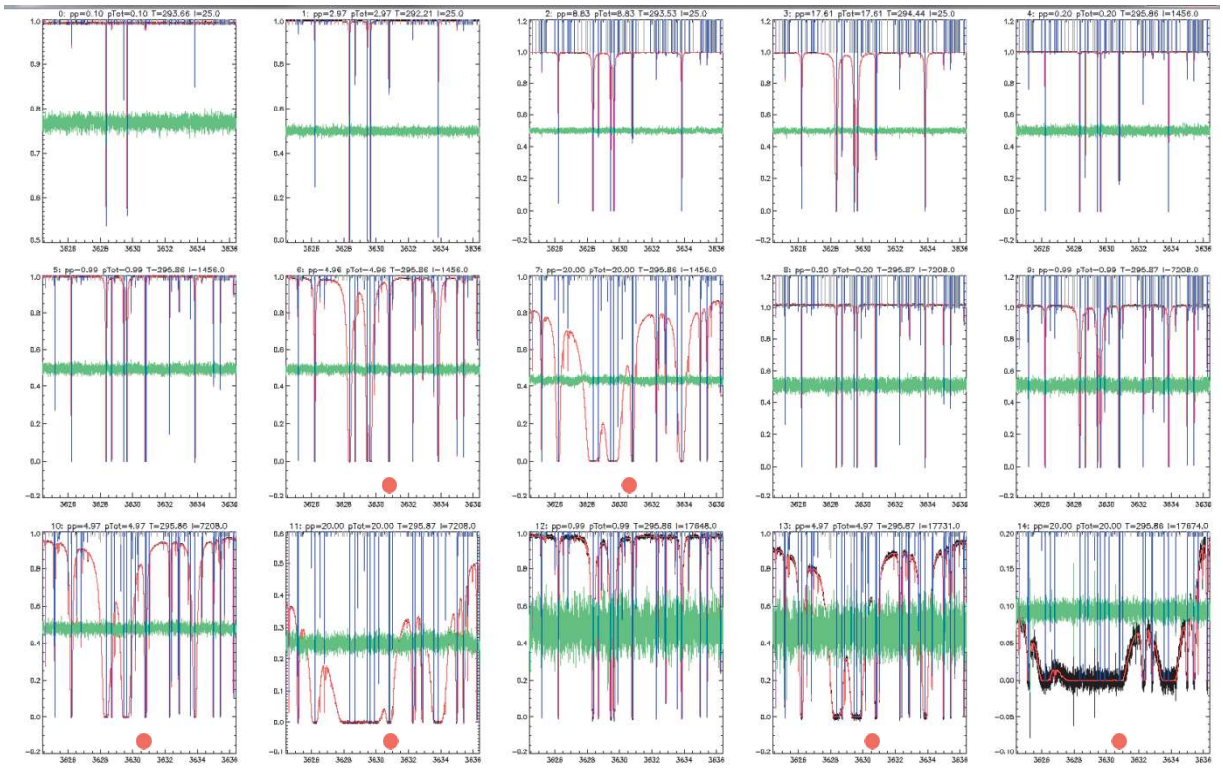

Figure 2. Screenshot of the multispectrum fit of the self broadening parameters in microwindow 3624.4-3636.4 cm^{-1}. Black: observed spectrum (mostly hidden beneath the red calculated spectrum), red:

calculated spectrum, green: (observed-calculated)x10 (shifted for better visibility), except last spectrum: (observed-calculated)x1, blue and grey: stick spectrum, stick length giving rough estimate of peak absorptance. Red dots indicate spectra/baselines used in the subsequent continuum fit. H_2O pressure [mbar], total pressure [mbar], temperature [K], and absorption path [cm] are noted above each graph and are listed in the same sequence in Table 2 in [Loos2017].

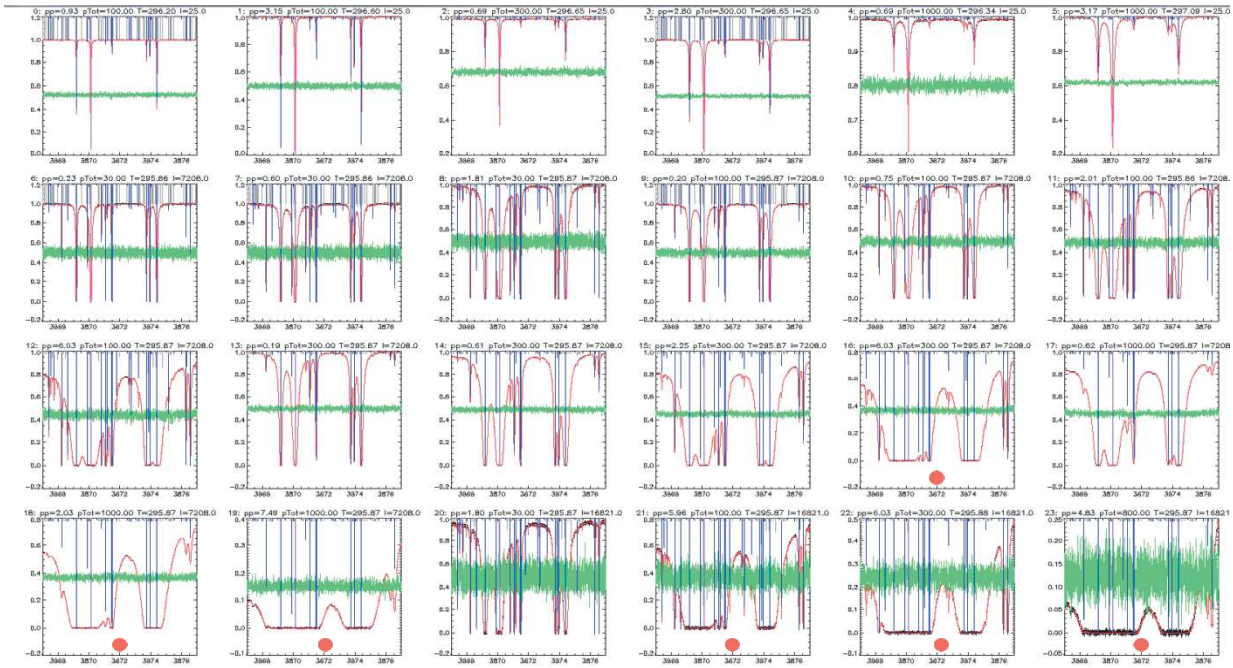

Figure 3. Screenshot of the multispectrum fit of the air broadening parameters in microwindow 3867-3877 cm^{-1}. Black: observed spectrum (mostly hidden beneath the red calculated spectrum), red: calculated spectrum, green: (observed-calculated)x10 (shifted for better visibility), blue and grey: stick spectrum, stick length giving rough estimate of peak absorptance. Red dots indicate spectra/baselines used in the subsequent continuum fit. H_2O pressure [mbar], total pressure [mbar], temperature [K], and absorption path [cm] are noted above each graph and are listed in the same sequence in Table 2 in [Loos2017a].

Figures 4 (self broadened) and 5 (air broadened) further illustrate the information flow from the spectra to the continua via the fitted baseline. The observed spectra are displayed as well as the modelled spectra from line parameters only, i.e. without continuum. Furthermore, the fitted baseline and the microwindow boundaries are shown. The visible red peaks contain the continuum information since the modelled spectra stand out from behind the observed ones at wavenumbers where continuum-induced

differences occur. It can be seen that most continuum information for the air-broadened measurements is close to the microwindow boundaries. In between, the baseline is linearly interpolated across the opaque regions which do not give any continuum/baseline information. The self-broadened data in Figure 4 shows more red than Figure 5 indicating more information due to the narrower lines and thus less extended opaque regions. The microwindow boundaries are not visible in the baselines in Figure 4 while they appear in Figure 5. The less congested self-broadened spectra allowed the use of small microwindows with a quadratic baseline, while the air-broadened spectra only allowed large microwindows with a linear baseline. The discontinuities visible in Figure 5 indicate errors in the fitted baseline and/or errors due to the linear representation of the baseline. The gap in the final baseline spectrum is caused by a too opaque spectrum throughout the microwindow.

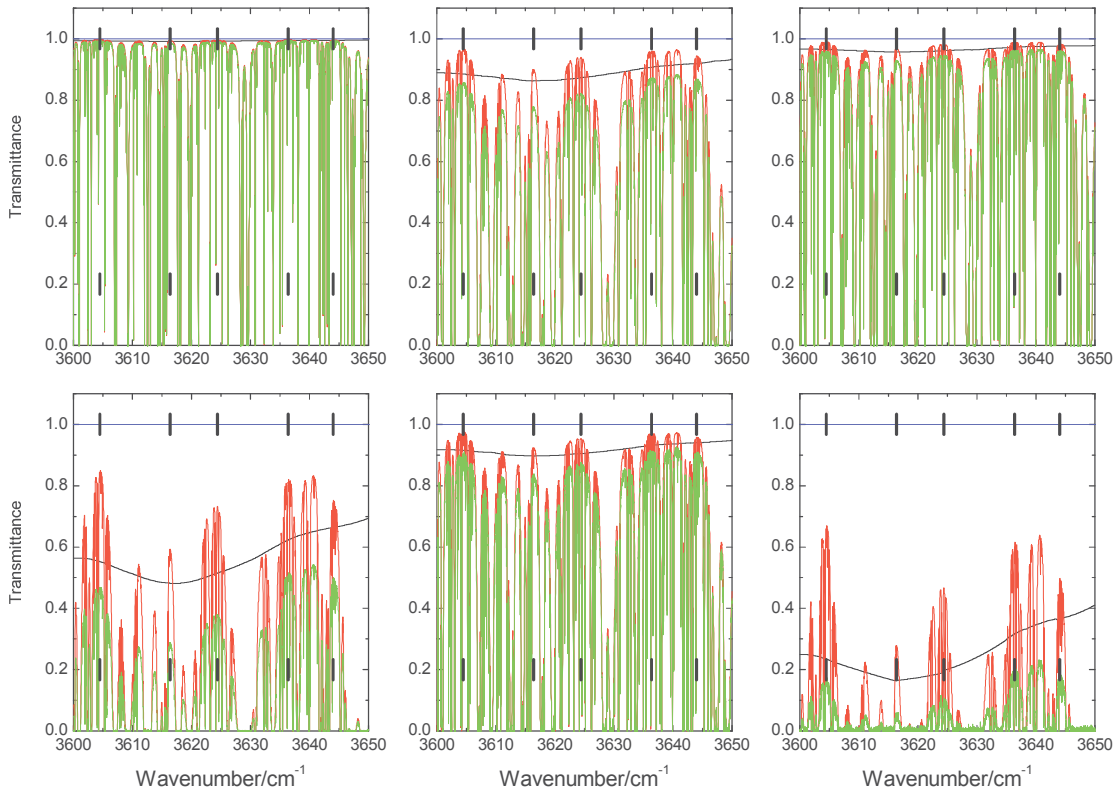

Figure 4. Transmittance contributions for SC determination from self-broadened spectra (Top left to bottom right: measurements 1-6 in Table 1). Green: observed spectra, red: modelled spectra from line

parameters only, black: fitted baselines, black sticks: microwindow boundaries, blue: 100% transmittance.

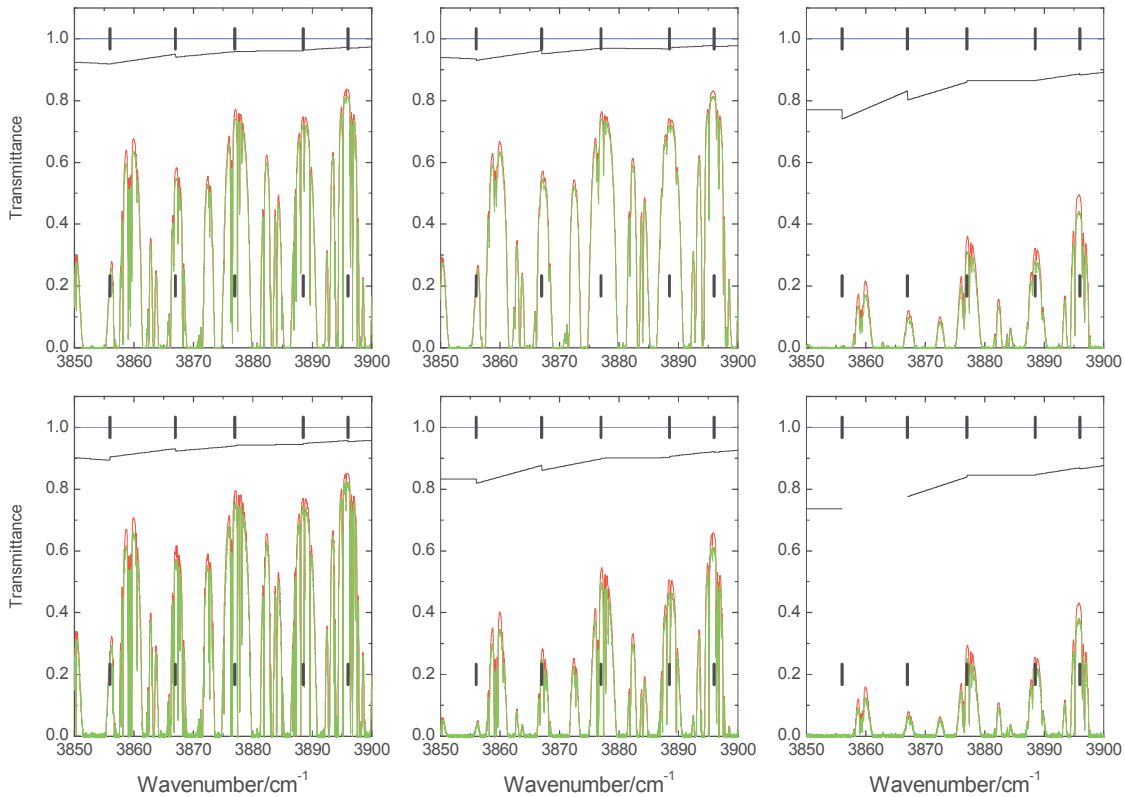

Figure 5. Transmittance contributions for continuum determination from air-broadened spectra (Top left to bottom right: measurements 7-12 in Table 1). Green: observed spectra, red: modelled spectra from line parameters only, black: fitted baselines, black sticks: microwindow boundaries, blue: 100% transmittance.

For the continuum analysis only spectra which have most information content regarding the continua were considered. Table 1 lists the relevant measurement conditions for these spectra. The continuum information content for each measurement, "IC_s" and "IC_f", are also listed in the table. In case of the SC we have $IC_s = p_{H2O}^2 \times l$ and in case of the FC $IC_f = p_{H2O} \times p_{tot} \times l$, where p denotes pressure and l the

absorption path. In addition to the information content it should also be taken into account that the FC according to MT_CKD (see above) is 12 times weaker. In the case of the SC and the pure H_2O measurements, it can be seen that two measurements (#4 and #6) are dominating the continuum information. In the case of the air-broadened measurements the information content for the SC is about 10 times smaller. The high temperature measurements have substantially less information and the disadvantage that SC and FC have to be fitted simultaneously.

Table 1: Measurements for continuum analysis. The list contains H_2O pressure, total pressure, absorption path, SC information content (IC_s), FC information content (IC_f), and baseline scaling correction factors (see section "Continuum fits"). The first block are pure H_2O measurements at 296 K, the second air-broadened measurements at 296 K and the third air-broadened measurements at 353 K.

#	p_{H2O}/mbar	p_{tot}/mbar	l/m	IC_s	IC_f	basecorrfact
1	4.9626	4.9626	14.50	350		1.001
2	20.0	20.0	14.50	5800		1
3	4.9651	4.9651	72.08	1773		1
4	20.0	20.0	72.08	28800		1
5	4.9655	4.9655	177.3	4354		0.994
6	20.0	20.0	176.7	70680		1
7	6.0	300	72.08	2592	129600	0.999
8	2.0	1000	72.08	288	144000	1
9	7.5	1000	72.08	4050	540000	1.005
10	6.0	100	168.21	6048	100800	1.001
11	6.0	300	168.21	6048	302400	1.003
12	4.8	800	168.21	3870	645000	1.002
13	0.6	100	72.08	26	4325	1.001
14	2.0	100	72.08	288	14416	1.002
15	5.7	100	72.08	2342	41086	1
16	17.3	100	72.08	21570	124700	1
17	0.6	100	168.21	61	10093	1.003
18	2.0	100	168.21	673	33642	1.004
19	6.0	100	168.21	6056	100926	1

2.3 Fitting procedure

The original transmittance spectra were inspected to assess the accuracy of the 100% level. The 100% baseline initially was not considered a relevant issue for the line parameter retrieval and the baseline polynomial coefficients contain the baseline fluctuations. Around 2600 cm^{-1} there were only few lines and the continuum was expected to have a contribution to the baseline of 0.2% (calculated from

MT_CKD3.2) for the largest information content for the SC. Thus, this region was assigned to 100% and the baseline coefficients were corrected accordingly.

It turned out that for the self-broadened measurements the baseline was nicely horizontal, thus for most measurements the 100% reference was useful for the 3400-4000 cm^{-1} region. In the case of air-broadened measurements, where the pressure was much larger than in case of the self-broadened measurements, the empty cell reference spectra were less valid. In this situation the baseline was bent for most measurements and the 100% reference was only useful for few measurements. Furthermore, the optical filter limits the range to 4000 cm^{-1} and the signal dropped substantially from 3900 to 4000 cm^{-1} leading to baseline problems in this region. Thus, the fitted continuum is not valid above 3900 cm^{-1}.

Software was developed to fit continua to the baselines. The scaled baseline segments were calculated from the second/first order polynomials on a 0.01 cm^{-1} grid. The baseline uncertainty was inferred from the statistical uncertainty of the 0th order baseline coefficient as determined from multispectrum fitting. The model functions for pure water and foreign broadened measurements are given in the following equations:

$$t_{base} = exp\left[-l \cdot (p_{H2O})^2 \cdot F \cdot C_s\right]$$

$$t_{base} = exp\left[-l \cdot (p_{H2O})^2 \cdot F \cdot C_s - l \cdot p_{H2O} \cdot p_{air} \cdot F \cdot C_f\right]$$

with t_{base} the baseline, *l* the absorption path in cm, p_{H2O} the water pressure in atm, p_{air} the air pressure in atm, F the conversion factor from pressure to number density @296 K (2.479×10^{19} molec $cm^{-3}atm^{-1}$), and C_s and C_f the self- and foreign-continuum coefficients in $cm^2molec^{-1}atm^{-1}$, respectively. The baselines of all relevant spectra were fitted simultaneously. These models ensure the quadratic p_{H2O} dependence of the SC absorption and the $p_{H2O} \cdot p_{air}$ dependence of the FC absorption. No systematic deviations from these models were observed.

2.4 Continuum fits

Three different fits have been performed.

Self-continuum from pure H_2O measurements

As described above the same narrow microwindows as in the original multispectrum fitting were used after improving the line parameter database to obtain narrow second order polynomial baseline

segments. Due to their high opacity, some baseline segments could not be fitted for some spectra leading to gaps. As described above large microwindows have less gaps and thus baselines of the large microwindows were used to fill the gaps. The final baselines appear noisy and were smoothed with a Gauss function of FWHM of 2.4 cm^{-1} except for the measurement with largest information content which still has gaps and the Gauss smoothing would decrease the available data substantially (convolution shortens available ranges by a half-kernel width). The kernel FWHM for this measurement was reduced to 0.5 cm^{-1}. Baseline correction scaling factors were applied to the observed baselines to reduce residuals in the region with most continuum information. The correction values are listed in Table 1. Only one measurement has a significant factor, but it is still well within 1% of unity. Observed and calculated transmittances are shown in Figure 6 together with the residuals. Beside the measurement #6 with maximum information content residuals are within 1%. The shapes of the residuals show baseline problems. The residuals show no specific dependence on pressure or absorption path and thus indicate the validity of fit model and input data. A further proof is the linear dependence of the optical depth on p_{H2O}^2. From the three pairs with the same pressures (see Table 1) the pair with the maximum absorption path and thus maximum information content was selected and $-\ln(t)/(p_{H2O}^2 l)$ formed. Figure 7 shows the good agreement between the 5 and 20 mbar measurements (#5 and #6 in Table 1) where p_{H2O}^2 differs by the considerable factor 16. The final result of the SC fit is shown in Figure 9.

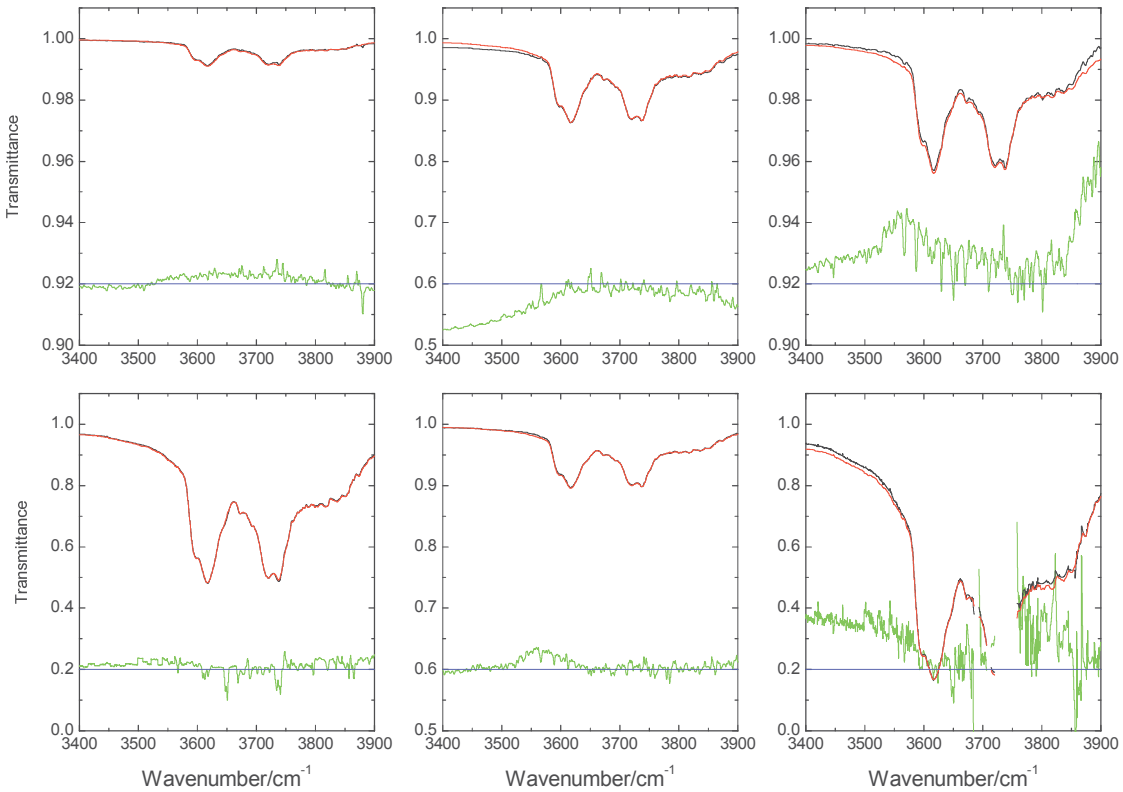

Figure 6. SC fit from pure H_2O measurements (from top left to bottom right measurements 1 to 6 in Table 1). Black: corrected observed baselines, red: calculated baselines, green: (observed-calculated) x 10, blue: zero line for green trace. Note the different transmittance scales among the plots.

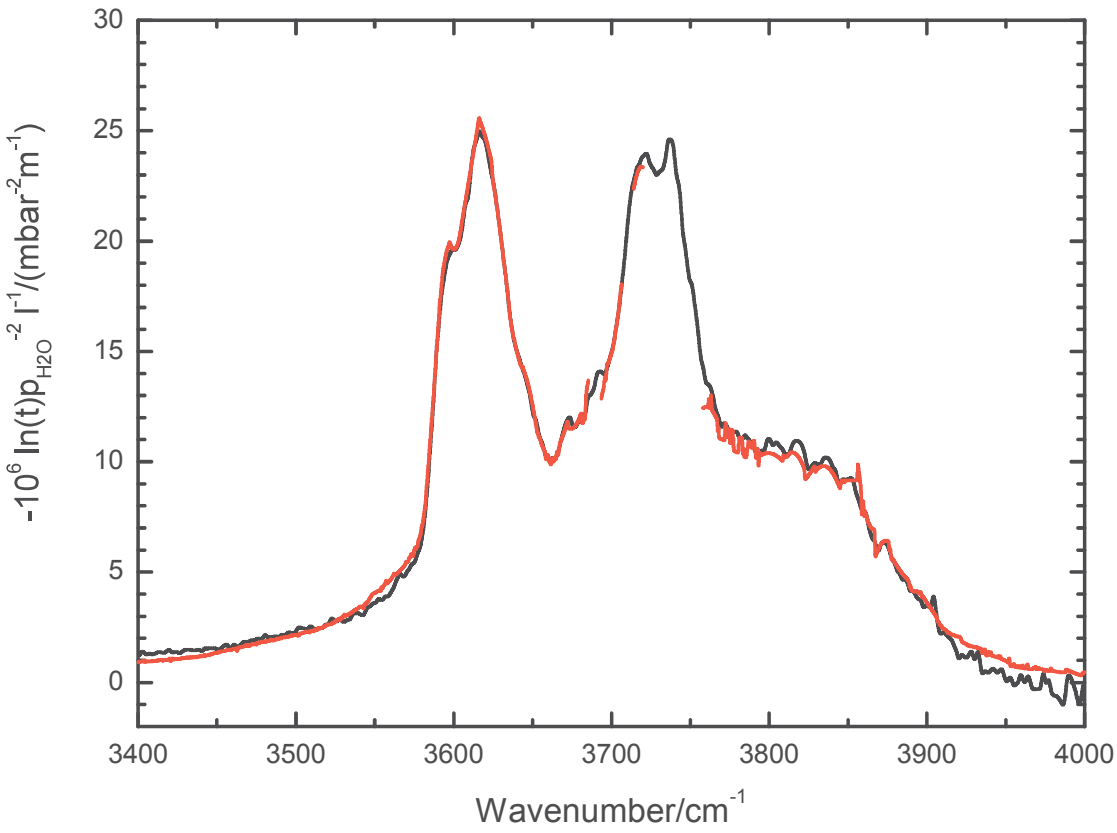

Figure 7. Validation of p_{H2O}^2 dependence of baseline optical depth. Black: 5 mbar, #5, red: 20 mbar, #6.

Foreign-continuum

In the FC case only wide microwindows were used as described above. The SC was inferred from the fit described in the last section and used to calculate its contribution in the transmittance spectra. As in the SC, baseline correction scaling factors were introduced to reduce residuals in the region with most continuum information. The correction values are listed in Table 1. In contrast to the SC case, only one measurement required no correction factor. Again, all factors are well within 1%. Observed and calculated transmittances are shown in Figure 8 together with the residuals. In addition, the contribution of SC and FC to the transmittance is shown. Although the FC is generally much larger than the SC, the SC still makes a substantial contribution and is the dominant contributor at some wavenumbers.

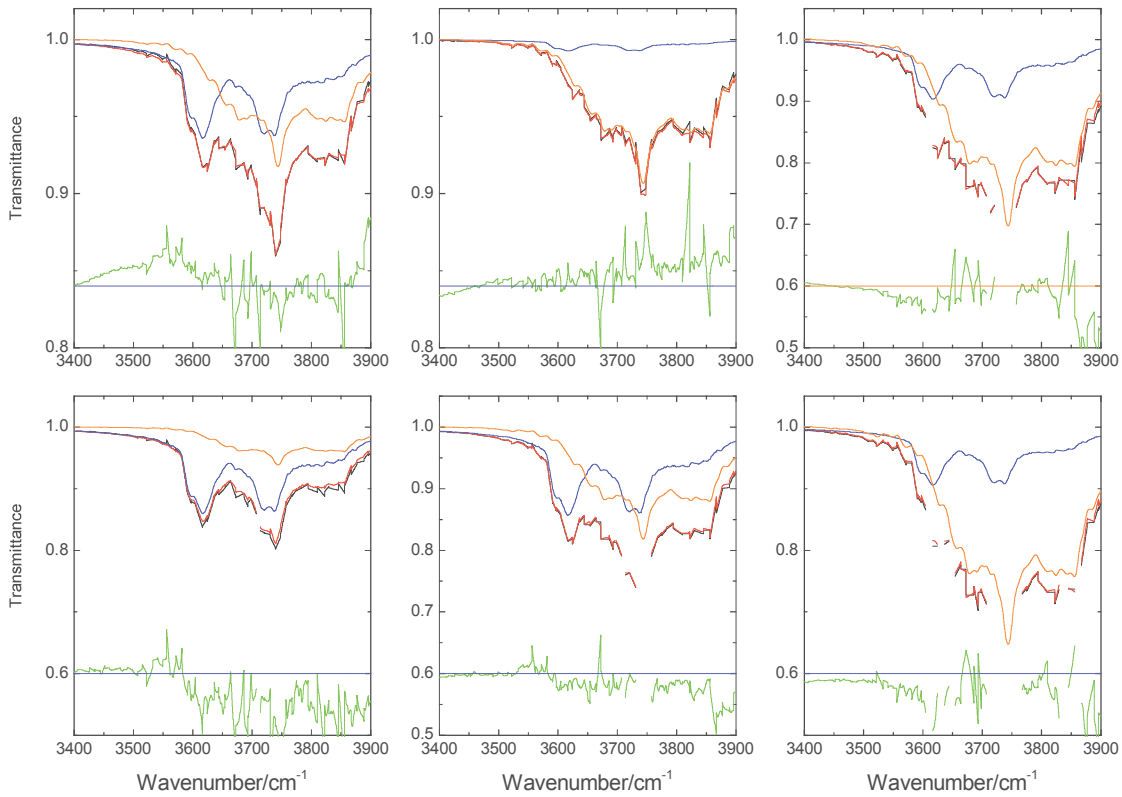

Figure 8. FC fit. Black: corrected observed baselines (from top left to bottom right measurements 7 to 12 in Table 1), red: calculated baselines, green: (observed-calculated) x 10, blue: transmittance of SC, orange: transmittance of FC, horizontal blue line: zero line for green trace. Note the different transmittance scales among the plots.

Fit of high temperature SC and FC

Unfortunately, there are no pure H_2O measurements at high temperature and furthermore, the maximum total pressure is 100 mbar only. Thus, it is not surprising that the information content of the continua (see Table 1) is much lower than for the room temperature measurements. SC and FC had to be fitted simultaneously. Due to the bad data quality uncertainties were not calculated.

3. Continua and error considerations

3.1 Self-continuum

As a consistency check, the self-continuum was also fitted using the air-broadened measurements only. The continua obtained from pure water measurements only and from air-broadened measurements only at 296 K are shown in Figure 9. The agreement is very good, showing that no additional errors are present. As expected, the SC retrieved from air-broadened measurements only is a bit noisy, also the spectral resolution is less since it is only based on the large microwindows. It can be seen that the SC is rather smooth without resolved structure although its resolution is rather high with a FWHM of mostly 2.4 cm^{-1}. The maximum relative change, which may be linked to a resolved structure, is around 3820 cm^{-1} and has an amplitude of 5%. Of course, this structure may be a result of the analysis and not real.

The largest error source for the continuum is the quality of the baseline. It was reported above that the baseline quality of the pure H_2O measurements was rather good and only two out of six baselines had to be scaled by factors deviating from unity by 0.1% and 0.6%, respectively. As a worst case it was assumed that the baseline knowledge is <1%. The baseline of measurement 4 was scaled by 0.99 and all other measurements were scaled to have similar residuals as in Figure 6. The fitted continuum was subtracted from the original one and the difference gives the uncertainty displayed in Figure 9. This method provides correlated errors only. The statistical uncertainties of the baselines yield an error <1% for the continuum. It was stated above that the maximum amplitude of structures with respect to the smoothed continuum is about 5%. A maximum relative error of this magnitude cannot be excluded. As a further quality check, residuals are calculated from the scaled measured transmittance spectra and modelled spectra calculated from the line parameters and the continuum, both derived from fitting. A first impression is given in Figure 10. The instrumental line shape was not included in the modelled spectra since the influence on the measured spectra is rather small. Furthermore, the calculation was carried out on a 0.01 cm^{-1} grid, which is much coarser than that of the original measurements. The residuals appear to be mostly noise beside a few spikes. These spikes were already in the measured transmittance spectra. There were contaminant lines in the measured data which were removed by fitting the contaminant spectra, calculating a transmittance and dividing the measured spectra by the calculated transmittance spectra. When the contaminant spectrum has zero transmittance, spikes occur from division of zero by zero. Details can be found in [Loos2017a]. The residuals of a smaller interval and - for intercomparison - the residuals of the multispectrum fitting are shown in Figure 11. Whereas the multispectrum fitting shows no residuals outside the noise level, there are some tiny residuals in the

calculation with the continuum. This is caused by the residuals in the continuum fitting (see Figure 6) together with the smoothing. However, these residuals are so small that the effect on the continuum is within the specified uncertainties and does not introduce additional systematic errors. These spectrally medium resolved residuals (features of about 1-2 cm^{-1} width, see Figure 11) should vanish when the multispectrum fitting is altered to fit continuum and line parameters simultaneously. Certainly, baseline errors will cause residuals in this fit but usually much wider.

The important conclusion is that, with the continuum and the line parameters determined from the same spectra, these spectra can be modeled close to the noise level. This also proves for the first time that the ν_1/ν_3 in-band SC is almost smooth at 2.4 cm^{-1} resolution. There are still high resolution features on the order of 5% of the local continuum value visible in the magenta curve in Figure 9, which we cannot distinguish from noise or artefacts.

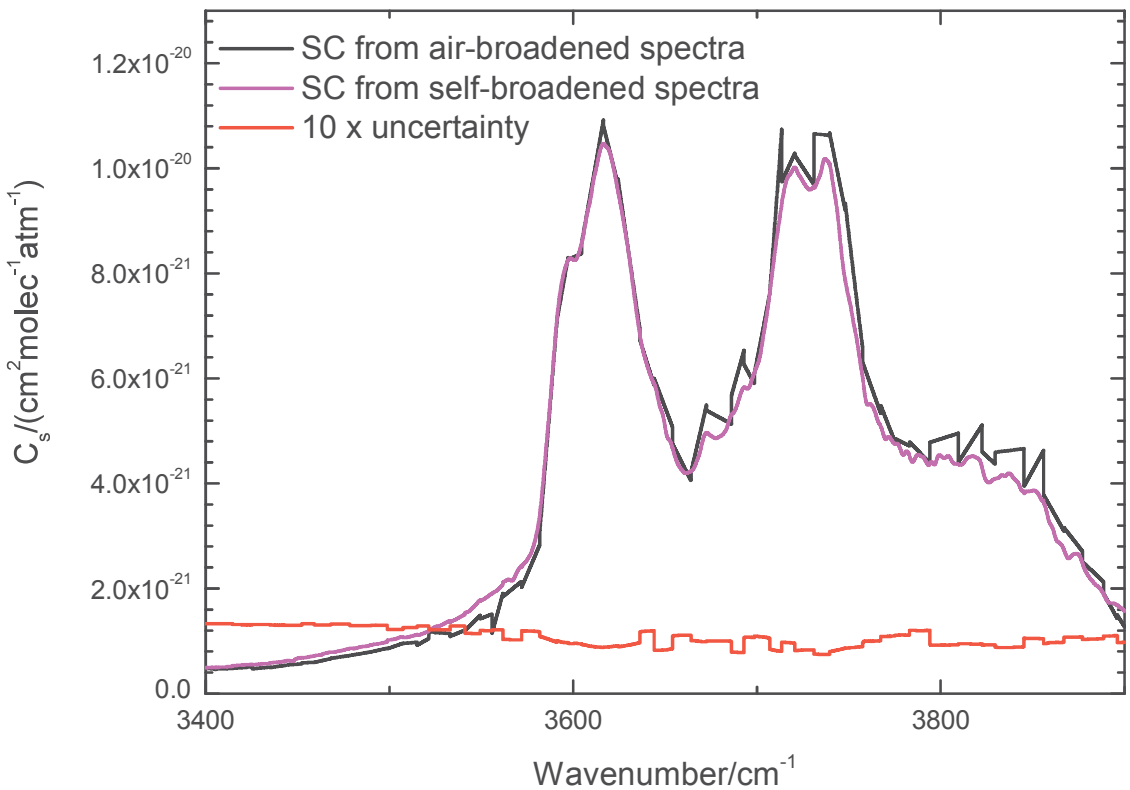

Figure 9. Fitted in-band SC from different measurements together with uncertainty for SC from self-broadened spectra.

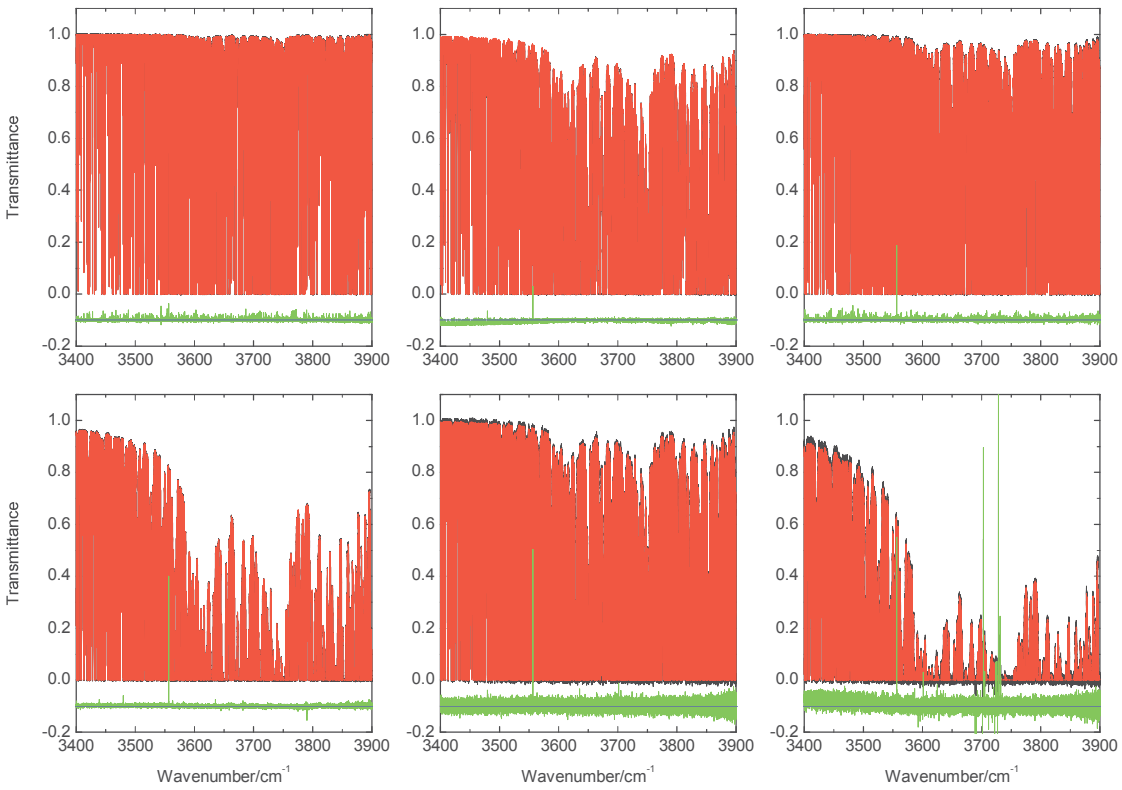

Figure 10. Measured spectra (from top left to bottom right measurements 1 to 6 in Table 1) and calculated spectra from fitted line parameters and SC. Black: measured spectra, red: calculated spectra, green: residuals (measured-calculated) x 2. Blue: zero line for green trace. For the spikes see text.

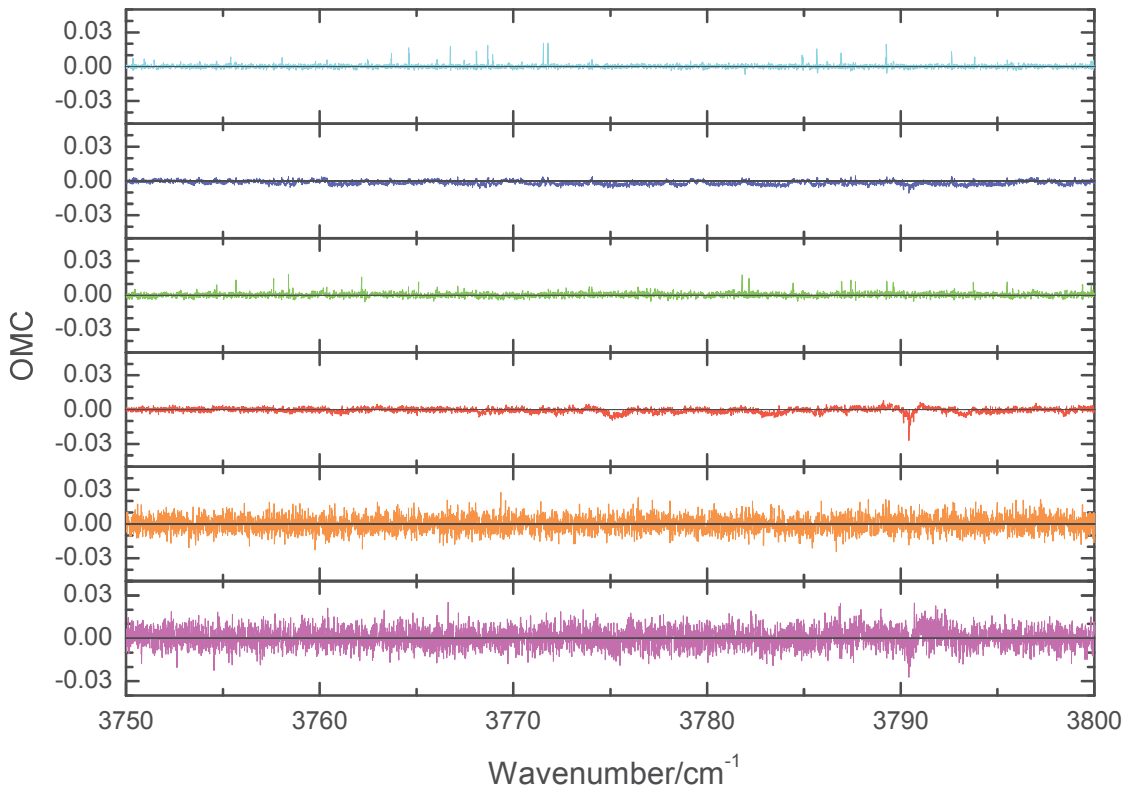

468

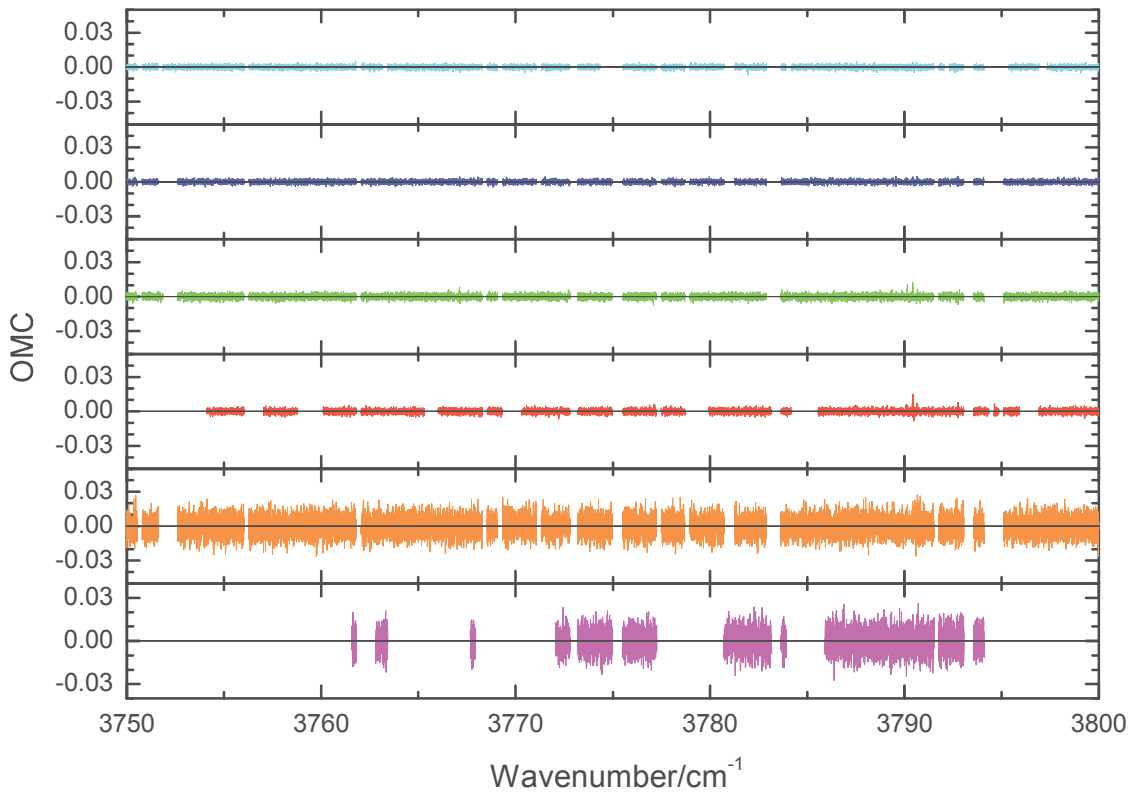

Figure 11. Top: excerpt of residuals (observed-calculated, OMC) from Figure 10, bottom: multispectrum fit residuals. Traces from top to bottom in each graph correspond to measurements 1 to 6 in Table 1. Note that the noise on top and bottom appears different due to the different point spacing (see text). Gaps in the bottom traces indicate that the corresponding spectrum was not included in the initial multispectrum fit. Non-noise residuals in the top graph show resolution of 1-2 cm^{-1} and amplitudes <1%. The spikes in 1st and 3rd trace top originate from the missing instrumental line shape in the model.

3.2 Foreign-continuum

The FC is shown in Figure 12. In contrast to the SC the analysis was carried out with baselines obtained from multispectrum fit with wide microwindows, as stated above. The wide linear baseline segments cause zigzag structures in the fitted continuum. Thus, Gauss smoothing was applied selecting σ as small as possible in order to remove the discontinuities. The selected Gauss FWHM of 7.2 cm^{-1} (corresponding to a Gauss σ of 3 cm^{-1}) was applied, and the results are also shown in Figure 12. The results for 353 K are shown for completeness, but due to the insufficient data (only foreign broadened measurements with single air pressure 100 mbar, see Table 1) the difference to 296 K may not be real, as can be seen from

the negative values around 3500 cm^{-1}. The error analysis was performed as described for the SC. The baseline of measurement 9 was scaled by 0.99 and all other measurements were scaled to have similar residuals as in Figure 8. The error is also displayed in Figure 12. The statistical error was <2% for most of the region 3600-3900 cm^{-1}. Residuals for the smoothed continuum were calculated for baselines and compared to the original residuals in Figure 8. For some spectra in some spectral regions, the residuals were increased which is not surprising since the original unsmoothed continuum from the fit should yield the optimal residuals.

As stated above, the microwindows were selected to have transmittance maxima at their borders, resulting in microwindow widths varying between 6 and 16 cm^{-1}. Certainly, this selection has an influence on the retrieved continuum. Alternative microwindow borders were chosen for the region 3800-3900 cm^{-1} still trying to use transmittance maxima as borders. The new borders were positioned approximately in the center of the old microwindows. Continuum fits were performed and the residuals were much larger than before. Clearly linear baselines work best when the borders are at transmittance maxima since then the linear interpolated baseline is feasible. The alternative microwindows mostly had lower transmittances at the borders and the linear baseline is less well determined. The fitted continuum showed more structure and had a maximum disagreement with the original one of 15% in a local region of 10 cm^{-1}. It is hard to specify an error on the relative continuum, i.e. how much structure is real, or whether the continuum is smooth. An estimated error of 15% is definitely too large and, given the differences of smoothed and unsmoothed continuum, 4% (average uncertainty given in Figure 12) is too small. Thus 10% is assumed as an approximate number.

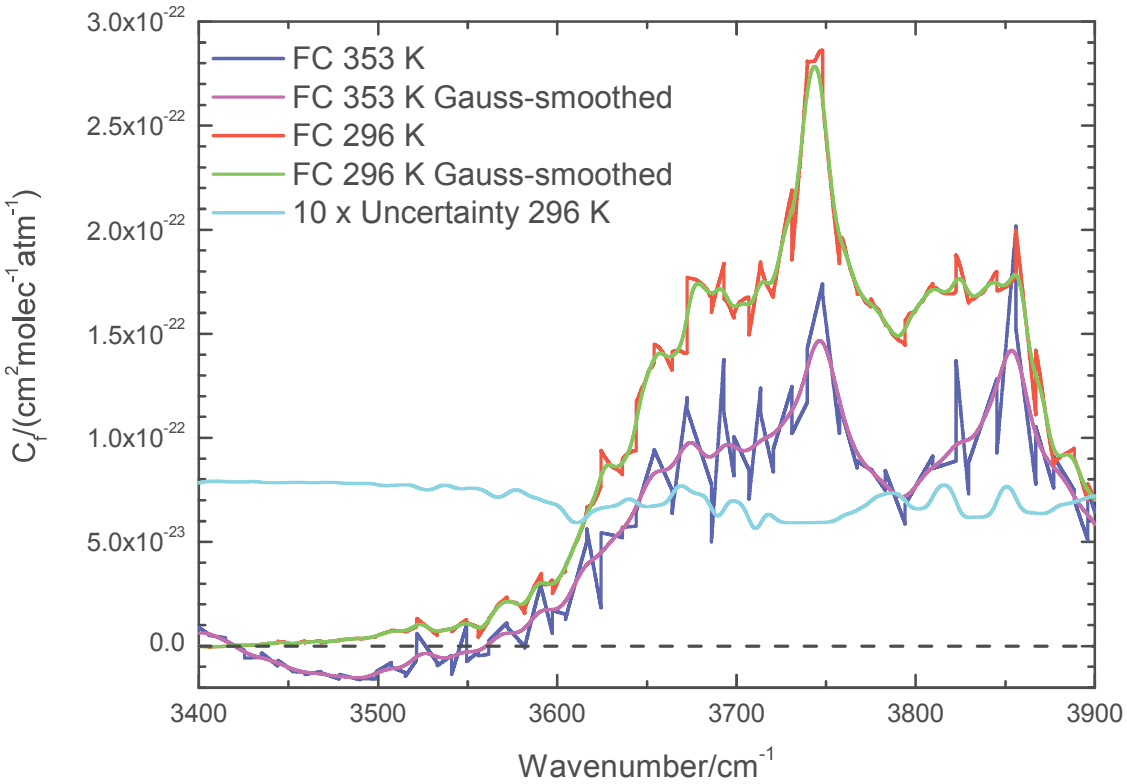

Figure 12. Foreign continua smoothed and unsmoothed at 296 K and 353 K together with uncertainty of 296 K continuum from baseline errors.

As in case of the SC, as a further quality check, residuals are calculated from the scaled measured transmittance spectra and modelled spectra calculated from the line parameters and the continuum. A first impression is given in Figure 13. Spikes are due to the missing ILS or due to opaque lines from contaminants as already explained for SC. Besides the spikes, the residuals look satisfactory. A more detailed view is given in Fig 14. In contrast to the SC where residuals of the multispectrum fitting are noise, in case of the FC small residuals outside the noise are present. The modelled spectra using the continuum show similar sized residuals as the multispectrum fitting. The unsmoothed continuum produces similar residuals. Again, as in case of SC, when continuum and line parameters were determined from the same spectra these spectra can be modeled close to the noise level. The inferred self-continuum also did not cause residuals, which was expected due to the good agreement shown in Figure 9. Note that the SC makes a substantial contribution to the air-broadened measurements as can be seen Figure 8.

The 296 K SC and FC together with the uncertainties can be found in the supplementary material.

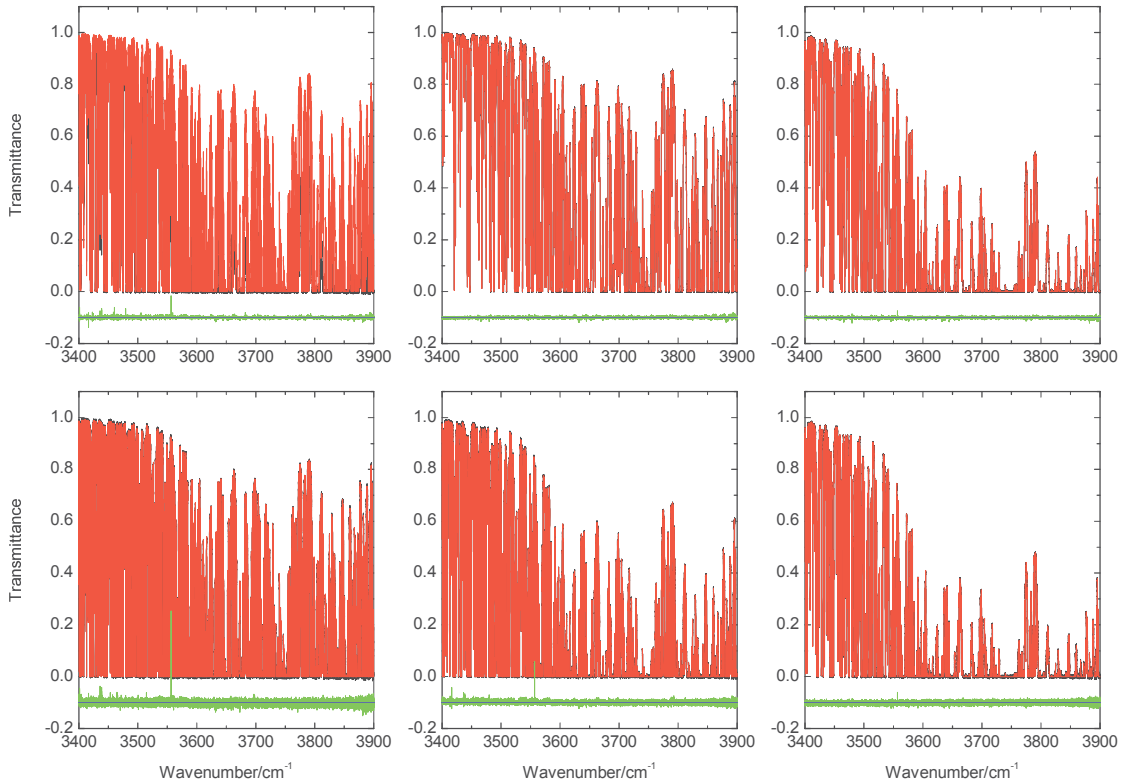

Figure 13. Measured spectra (from top left to bottom right measurements 7 to 12 in Table 1) and calculated spectra from fitted line parameters, FC, and SC. Black: measured spectra, red: calculated spectra, green: residuals (measured-calculated) x 2. Blue: zero line for green trace. For the green spikes see text.

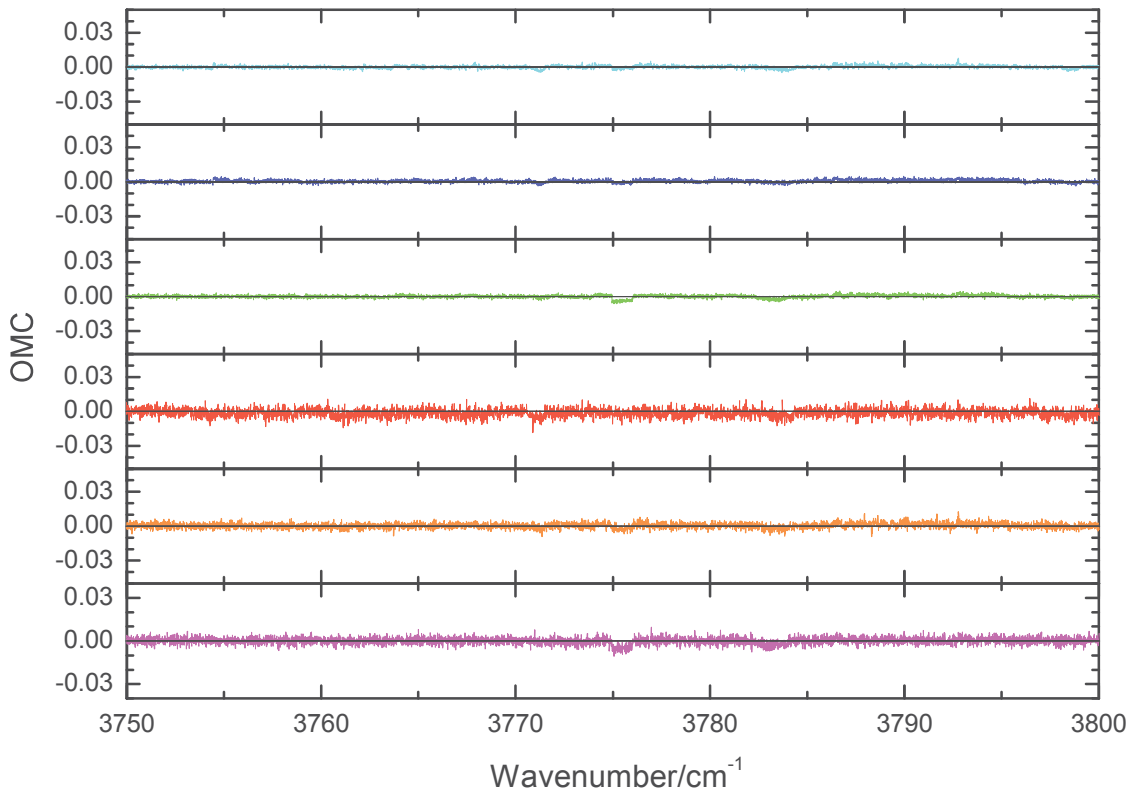

527

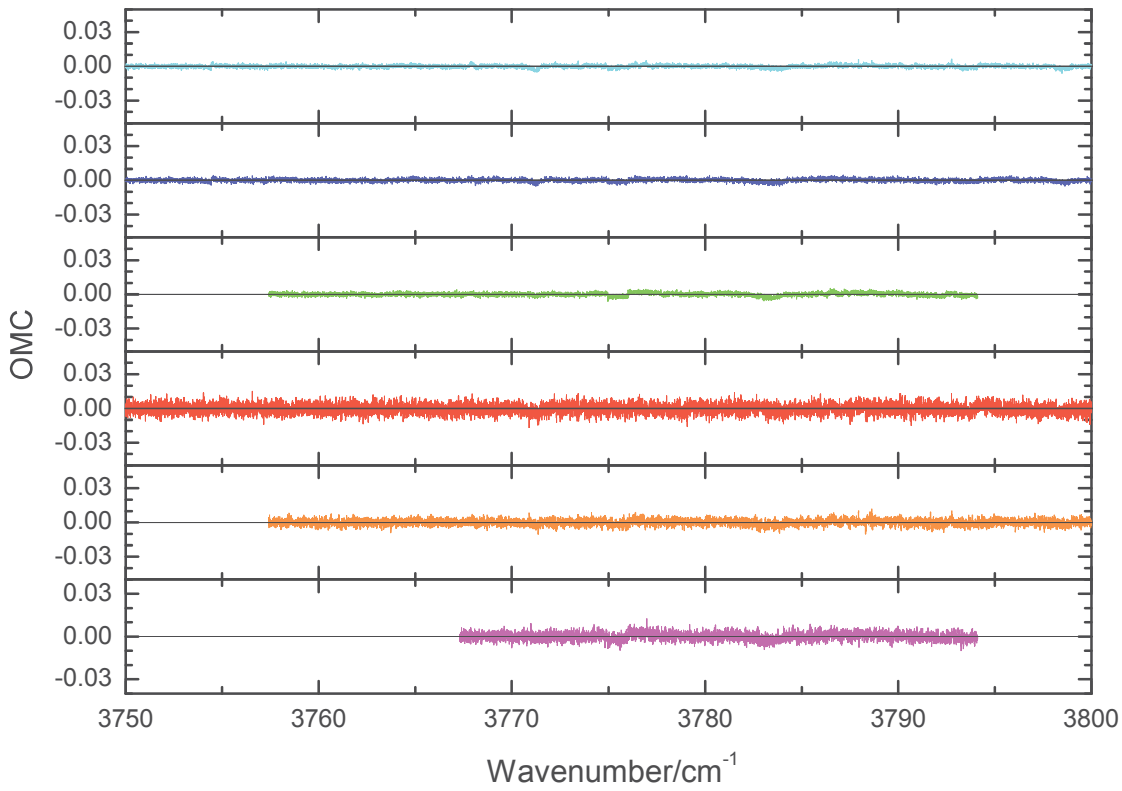

Figure 14. Top: excerpt of residuals (observed-calculated, OMC) from Figure 10, bottom: multispectrum fit residuals. Traces from top to bottom of each graph correspond to measurements 7 to 12 in Table 1. Note that the noise on top and bottom graphs appears different due to the different point spacing (see text). Gaps in the bottom traces indicate that the corresponding spectrum was not included in the initial multispectrum fit.

4. Analysis of self-continuum

4.1 Shape of bound dimer bands

The positions and intensities of the H_2O dimer fundamentals have been studied in *ab initio*, e.g. [Kjaergaard2008] and experimental work, e.g. [Ceponkus2008,Kujanov-Prozument2010]. In the 3 µm region there are four fundamentals. Forming averages among the cited studies shows that the positions and intensities of the three stronger fundamentals agree within ±20 cm^{-1} and ±20% (1σ), respectively.

[Ptashnik2011] simulated the dimer spectrum based on VPT2 in [Kjaergaard2008] assuming the dimer bands to be simple Voigt profiles with 60 cm^{-1} FWHM, which is a very approximate estimate of a band envelope. In [Ptashnik2019] most of the fundamentals were taken from [Kujanov-Prozument2010] and two fundamentals shifted to better match the observed continuum. In an older *ab initio* work [Tso1998] calculated the rovibrational spectrum of the dimer between 0 and 20000 cm^{-1}. We found too large differences to the observed continuum to use the results in this investigation.

In the following the expected rovibrational spectrum of the H_2O dimer in the 3 µm region will be discussed. The B and C rotational constants are about equal, approximately 0.2 cm^{-1} and the A rotational constant is about 7 cm^{-1} [Mukhopadhyay2015]. The H_2O dimer is a nearly prolate top molecule. Because of the much higher moment of inertia, the rotational constants are significantly smaller when compared to the monomer with C≈9 cm^{-1}, B≈15 cm^{-1}, A≈28 cm^{-1}. This difference has a large impact on the shape of the dimer bands when compared to the monomer bands. There are three strong rovibrational bands in the 3 µm region. The band around 3597 cm^{-1} is the dimer fundamental ν_3 which corresponds to the symmetric OH stretch of the donor H_2O [Kjaergaard2008]. The axis with the smallest moment of inertia (A-axis) is nearly parallel to the H-bridge OH donor bond and close to both O atoms. The donor symmetric OH stretch changes the dipole moment both parallel and perpendicular to the A-axis and therefore the rotational structure should show both the parallel and perpendicular band of a prolate symmetric top molecule (see [Herzberg1945], Fig 122 and Fig 128, respectively). For the dimer fundamental ν_1, corresponding to the ν_3 of the donor H_2O around 3730 cm^{-1}, the vibration changes also both the dipole moment parallel and perpendicular to the A-axis. In contrast to this the ν_9 around 3749 cm^{-1} (antisymmetric OH stretch of the acceptor H_2O) changes the dipole moment only perpendicular to the A-axis. Rotationally resolved ΔK_a=1 transitions in the ν_9 were observed by [Huang1988,Huang1989] confirming the perpendicular band type. It should be mentioned that the rovibrational band types were also derived in [Huang1989]. In contrast to [Kjaergaard2008] the donor symmetric and asymmetric O-H stretches were treated as localized “bonded” and “free” O-H stretches, respectively. This would lead to almost parallel and perpendicular bands, respectively. As shown later, both bands have about similar parallel and perpendicular contributions, more in line with the vibrational modes as described by [Kjaergaard2008]. Furthermore, in [Huang1989] the “bonded” O-H stretch has a band center at 3545 cm^{-1} which is in contradiction to [Kjaergaard2008].

Due to the five low lying fundamentals only 14% of the 3 µm vibrational bands originate from the ground state. The rest is distributed among about 20 hot bands, with different rotational and centrifugal

distortion constants and band centers. Due to the slightly asymmetric top an asymmetry splitting exists decreasing with increasing K_a. The H_2O dimer exhibits three tunneling motions leading to a sixfold splitting, the largest about 12 cm^{-1} (see [Mukhopadhyay2015] and references therein and [Cole2015]). The splittings change with vibrational state and rotational quantum numbers. The molecule dissociates from the excited vibrational states belonging to the 3 µm bands leading to lifetime broadening which depends on the individual state [Huang1989]. The complex pattern can be seen even at the low temperatures of the rotationally resolved molecular beam spectrum of the librational band in the 20 µm region (Figure 2 in [Cole2015]). To find resolved rotational structure at room temperature appears to be unlikely. However, in case of pure rotation some so-called E-type transitions are not much affected by the tunneling splittings and form regular 2B-spaced patterns which were observed in ambient temperature water spectra [Tretyakov2013;Serov2014;Koshelev2018] and modelled by [Odintsova2014]. Anyhow, the typical shape of a parallel or perpendicular band should approximately be maintained for individual rovibrational bands.

In order to model the expected shape of the dimer parallel and perpendicular bands individual rovibrational lines were modelled. Line positions and relative intensities were calculated according to Chapter IV.2 in [Herzberg1945] applying the abovementioned rotational constants ignoring centrifugal distortion and vibrational dependence of rotational constants. In order to account for effects mentioned in the last paragraph causing a rather congested, unresolved spectrum each line was modelled as a 5 cm^{-1} HWHM for the parallel and 10 cm^{-1} HWHM Lorentzian for the perpendicular band. This selection was made to smear out individual Q branches in the perpendicular bands and to best approximate the shape of the two narrow features in the observed continuum by the parallel bands. The parallel and perpendicular band shape kernels were assumed to be the same for all rovibrational bands.

A more sophisticated method for obtaining rovibrational spectra of the dimer is using *ab initio* calculations involving potential energy and dipole moment surfaces. For the region below 500 cm^{-1} the entire rovibrational spectrum was modelled with this method (see Figure 10 in [Scribano2007]). [Odintsova2019] measured the FIR SC below 50 cm^{-1} and found good agreement with the dimer prediction from [Scribano2007]. Based on the band centers and intensities of the low-lying dimer fundamentals [Kjaergaard2008] we simulated the spectrum using our simplified approach and found coarse agreement regarding overall shape. Certainly, the quality of the *ab initio* calculation depends on the availability of adequate potential energy and dipole moment surfaces. Therefore, the older *ab initio* calculation cited above [Tso1998] with many approximations shows disagreement with the experimental continuum data.

4.2 Fit of self-continuum contributions

As in [Ptashnik2019] the continuum was fitted as the sum of a quasi-bound dimer spectrum and a bound dimer spectrum. The quasi-bound dimer spectrum contribution is modelled from the monomer line positions and intensities given in HITRAN2016 [Gordon2017] (which in turn are taken from [Loos2017]). Ptashnik et al. [Ptashnik2011] estimated from lifetimes that the FWHM should be in the range 14-40 cm^{-1}. The FWHM for the calculation of the quasi-bound dimer from the monomer spectrum in the [Ptashnik2011] and [Ptashnik2019] work was 20 cm^{-1}. We decided to use two cases, FWHM=20 and 40 cm^{-1}. The bound dimer was modelled from band centers and total band intensities where ν_1 and ν_3 were mixed parallel and perpendicular bands and ν_9 purely perpendicular. The kernels described in Section 4.1 were used. The weak ν_2 band was not fitted. It was assumed that the parallel band contribution is 0.5. The integral intensity of the four bands was calculated by averaging the experimental value for Ne matrix in [Ceponkus2008], the experimental value from [Kujanov-Prozument2010], and the theoretical value VPT2 from [Kjaergaard2008]. The mean value was $4.90(41)\times10^{-17}$ cm^2cm^{-1}/molec, where the uncertainty is the maximum difference to the mean. The initial guess for the partitioning of the intensities among the three fundamentals is taken from the averaging and that for the band centers from [Ptashnik2019]. The fractions for ν_3 and ν_1 are used as fit parameters while the fraction for the ν_9 is calculated since the sum of all fractions is 1.

The continuum calculation involves the constants K_{Db} and K_{Dq}. The sum of both constants yields the total dimerization constant K_{eq}. The constants, band centers, intensity partitioning and the fraction of parallel bands, fpara, for ν_1 and ν_3 can be fitted. The sum of parallel and perpendicular fractions is 1. The fit results are summarized in Table 2. The statistical uncertainties were too small to be meaningful and thus omitted, considering all the assumptions and approximations. The literature values for the intensity fractions and the band centers are given in the last row. In cases #1 and #2 all parameters were fitted. While in case #1 the FWHM of the Lorentz line shapes was 20 cm^{-1} it was 40 cm^{-1} in case #2. The fitted values agree reasonably with the literature, except for the fraction $fS_{\nu9}$ in case #1 and the vibrational band centers of the ν_9 being unphysically high. The dimer fundamentals associated with OH stretching vibrations should be below the monomer values which is in case of the ν_9 dimer band the monomer ν_3 band center at 3756 cm^{-1} [Kjaergaard2008]. Indeed, the value used by [Ptashnik2019], a result of [Kujanov-Prozument2010], is 3749 cm^{-1} which is slightly lower than the monomer value. In case #3 we fixed the band center of the ν_9 to 3749 cm^{-1}. The fitted parallel contribution of ν_1 was above 1 which is unphysical, furthermore, the intensity of the ν_1 is too small and that of ν_9 way too large.

Following [Kjaergaard2008] treatment of the vibrations on the basis of donor ν_1 and ν_3 the dipole moment changes with vibration are orthogonal. Assuming that the H-O-H angle of the donor is around 104° and the A axis is approximately parallel to the nearly linear O-H-O frame the direction of the dipole moment change has an angle of 52° to the A axis for the donor ν_1 and 38° for the donor ν_3. This would imply a somewhat greater parallel than perpendicular band contribution for the donor ν_3. In cases #4 and #5 $fpara_{\nu 1}$ was fixed to 0.6. The fitted band intensity (see Table 2) of ν_3 agrees reasonably with the literature value (max. difference 13%), and that of ν_1 even better (max. difference 7%). The weakest band (ν_9) among the three considered fundamentals is the worst case, and is 39% stronger than the literature value which is somewhat outside its uncertainty.

In cases #6 and #7 the Lorentzian HWHM for the parallel and perpendicular band kernels were doubled. Note that the HWHM for the perpendicular band is a minimum value while for the parallel band it is an approximate optimal value. The doubling should give an estimate of the sensitivity of the fit to these HWHM values. The agreement of the band intensity fractions with literature is worse than for the cases with nominal HWHM. Anyhow, FWHM qD has a larger impact on the dimerization constants than the Lorentzian HWHM of parallel and perpendicular bands.

Figure 15 shows the observed, calculated, the residuals and the individual contributions to the continuum as well as the calculated bound dimer spectrum for two cases, #1 giving the best residuals, and #4 with larger residuals but physically meaningful parameters. It is remarkable that the residuals in case #1 above 3740 cm^{-1} are very small. The two double maxima of the continuum are clearly linked to the P- and R-branch structure of the respective parallel bands. The constants K_{Db}, K_{Dq}, and K_{eq} were averaged for the cases #4-#7 since they do not contain unphysical results and contain the impacts of changing both the quasi-bound and the bound dimer rovibrational band shapes. Resulting averages are K_{Db}=0.026(2) atm^{-1}, K_{Dq}=0.044(5) atm^{-1}, and K_{eq}=0.070(4) atm^{-1}. The uncertainties given in parentheses reflect only the variation for the selected model changes and are thus a rough estimate. Regarding the well-known K_{eq}=0.052 atm^{-1} [Ptashnik2019] the value is too high by 0.018 atm^{-1}. One possible error source is the total band intensity of the bound dimer in the spectral region of interest being too small in the calculations of Kjaergaard [2008]. Indeed, the total band intensity could be too small since some combination bands (with fundamentals <300 cm^{-1}) not accounted for in the calculations may exist in the relevant spectral range. However, an increase of the total band intensity by an unrealistically high value of 50% would decrease K_{eq} only by 0.008 atm^{-1}.

An alternative possibility is that 41% of the quasi-bound dimer contribution, corresponding to the 0.018 atm^{-1} excess, is caused by middle wing super-Lorentzian effects as suggested by [Serov2017]. This continuum contribution is a factor 6 larger than the foreign-continuum (see Figure 15), as calculated from the areas of SC super-Lorentzian contribution and FC. Let us assume that the in-band FC and the SC contributions have the same physical origin which can be described as super-Lorentzian (see Section 5.2). Assuming further that the middle wing super-Lorentzian effect scales the same way as the Lorentz widths when comparing self and foreign Lorentz broadening ($\gamma_{self} \approx 5 \cdot \gamma_{air}$), the super-Lorentzian self-continuum contribution should be about 5 times larger than the foreign-continuum. This is indeed comparable to the abovementioned factor 6. Presumably, the middle wing super-Lorentzian contribution has a slightly different shape when compared to the quasi-bound dimer spectrum. In case the shape was similar to the foreign-continuum it could be narrower than the quasi-bound dimer spectrum (see Figure 19). We modified the fitting software and mixed 59% of the quasi-bound dimer spectrum with 41% of the FC which was scaled to the area of the quasi-bound dimer spectrum. The fitted results and residuals were similar to the results obtained with the pure quasi-bound dimer spectrum. This shows that in case the middle wing super-Lorentzian contribution of the SC has the same shape as the FC this has only a small influence of the present results. The findings support the proposed presence of middle wing super-Lorentzian monomer contributions. The true dimerization constant, KDq', for the quasi-bound dimer should then be 0.026 atm^{-1} (0.044 atm^{-1} – 0.018 atm^{-1}).

The results should be regarded with care since the band shapes are still a crude approximation neglecting, as mentioned above, hot bands, tunneling splitting, centrifugal distortion, and asymmetry splitting. Furthermore, some weak combination bands are missing. The unphysical solutions of the fit may be linked to such approximations. The larger residuals close to the parallel band centers also show the limitations. In order to calculate approximate experimental dimer spectra the constants K_{Db} and K_{Dq} were fixed to the averages and all other parameters fitted for both FWHM qD cases. The fitted results are listed in cases #8 and #9 in Table 2. A further approximation is to assume the quasi-bound dimer spectra to look exactly as a broadened monomer spectrum. In reality the spectrum of the quasi-bound dimer can be expected to be something in-between bound dimer and monomer spectra, since close to dissociation the distance between the two water molecules increases. Certainly, *ab initio* calculations can cover bound and quasi-bound states, although the transition to two monomers is a challenge. [Scribano2007] did his *ab initio* calculation up to the dissociation limit including several approximations. It is expected that the calculated spectrum already contains some quasi-bound contributions.

Table 2. Fit results of SC for cases discussed in the text. Blue bold and black numbers indicate fitted and fixed parameters, respectively. K_{Db} and K_{Dq} are the equilibrium constants for the bound and quasi-bound dimer respectively, with K_{eq} being the sum of these. fSs show the fraction of the total intensity which is assigned to each of the three fundamental bands of the bound dimer, assuming that all the intensity is due to these bands, excluding the weak fundamental. fpara is the fraction of the intensity in each band which is assigned to the contribution to the parallel component (the remainder being due to the perpendicular component – the nu_9 band is assumed to be entirely perpendicular). The fitted band centres for each of these bands is given by nu_o. The assumed full-width half maximum of the quasi-bound dimer contribution is given by FWHM qD. The table has three sections separated by horizontal lines. The first section contains the nominal fits, in the second section the HWHM for the Lorentzian line widths in the parallel and perpendicular dimer bands were doubled, in the lowest section the constants K_{Db} and K_{Dq} were fixed to results obtained in the first section.

#	**K_{Db} /atm^{-1}**	**K_{Dq} /atm^{-1}**	**K_{eq} /atm^{-1}**	**$fS_{\nu3}$**	**$fS_{\nu1}$**	**$fS_{\nu9}$**	**$fpara_{\nu3}$**	**$fpara_{\nu1}$**	**$\nu_{0,\nu3}$ /cm^{-1}**	**$\nu_{0,\nu1}$ /cm^{-1}**	**$\nu_{0,\nu9}$ /cm^{-1}**	**FWHM qD /cm^{-1}**
1	**0.029**	**0.035**	0.064	**0.48**	**0.21**	0.31	**0.44**	**0.83**	**3611**	**3724**	**3765**	20
2	**0.027**	**0.040**	0.067	**0.48**	**0.30**	0.22	**0.47**	**0.60**	**3611**	**3726**	**3780**	40
3	**0.031**	**0.039**	0.070	**0.44**	**0.12**	0.44	**0.44**	**1.25**	**3611**	**3723**	3749	20
4	**0.025**	**0.042**	0.067	**0.48**	**0.27**	0.25	**0.54**	0.6	**3610**	**3724**	3749	20
5	**0.024**	**0.050**	0.074	**0.49**	**0.30**	0.21	**0.55**	0.6	**3610**	**3726**	3749	40
6	**0.028**	**0.038**	0.066	**0.42**	**0.32**	0.26	**0.76**	0.6	**3611**	**3724**	3749	20
7	**0.026**	**0.047**	0.073	**0.43**	**0.36**	0.21	**0.78**	0.6	**3611**	**3725**	3749	40
8	0.026	0.044	0.070	**0.47**	**0.35**	0.18	**0.52**	**0.51**	**3610**	**3724**	**3776**	20
9	0.026	0.044	0.070	**0.49**	**0.31**	0.20	**0.49**	**0.61**	**3611**	**3726**	**3776**	40
lit				0.55(8)	0.28(6)	0.18(3)			3597	3730	3749	

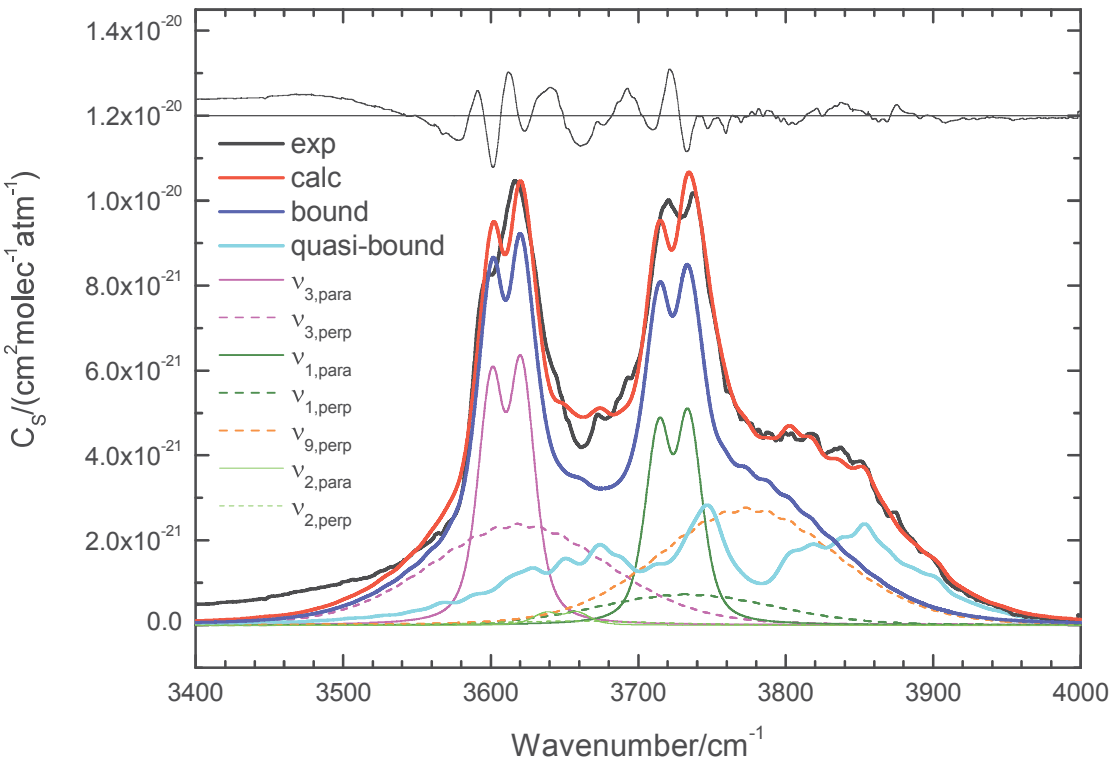
1.4x10-20
1.2x10-20
1.0x10-20
8.0x10-21
6.0x10-21
4.0x10-21
2.0x10-21
0.0
Cs/(cm2molec-1atm-1)
exp
calc
bound
quasi-bound
ν3,para
ν3,perp
ν1,para
ν1,perp
ν9,perp
ν2,para
ν2,perp
3400
3500
3600
3700
3800
3900
4000
Wavenumber/cm-1

711

712

713

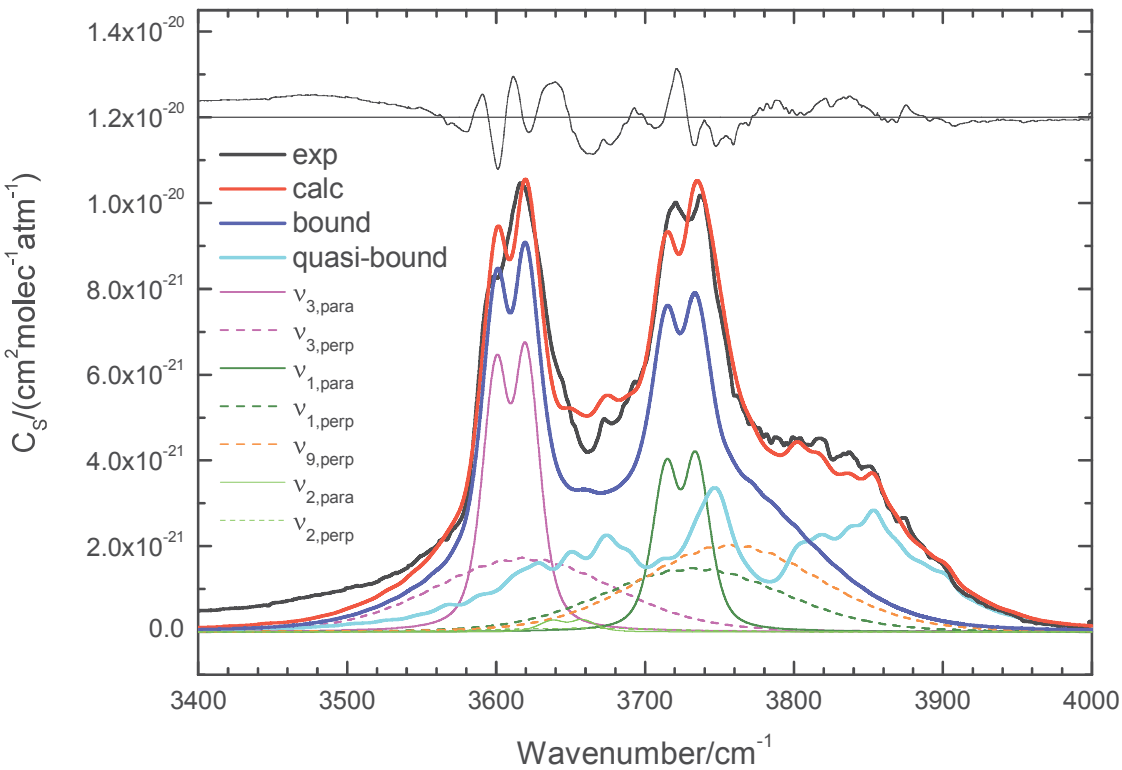

Figure 15. Observed and fitted SC at 296 K. Top: case #1 in Table 2, bottom: case #4 in Table 2. Thick black: Observed SC, thick red: calculated SC, thick blue: sum of bound dimer contributions, thick cyan: quasi-bound dimer contribution, magenta, green, orange, light green: ν_3, ν_1, ν_9, ν_2 bound dimer contributions. The four broad features are perpendicular bound dimer bands (dashed) while the narrower double-peak features are parallel bound dimer bands (solid). Note: The ν_9 has only a perpendicular contribution. Residuals of the fit offset by 1.2×10^{-20} $cm^2molec^{-1}atm^{-1}$ are shown in black.

5. Discussion

5.1 Self-continuum

Comparison with other work

The SC for 296 K and 353 K is compared to the CAVIAR work for 293 K and 351 K ([Paynter2009], downloaded from http://www.met.reading.ac.uk/caviar/home/data.php) and to MT_CKD3.2 in Figure 17. There are further experimental data cited in Section 1.4. Comparison of these earlier data with the

CAVIAR work can be found in Figure 6 in [Paynter2009] and in Figure 2 in [Ptashnik2019]. The CAVIAR 293 K SC is in good agreement with the present data between 3600 and 3800 cm^{-1}. However, inspection of the uncertainties and the differences between the present work and [Paynter2009], shown in Figure 18, exhibits significant discrepancies at both higher and lower wavenumbers. The uncertainties of the present work are up to a factor 20 smaller above 3550 cm^{-1}, especially in the intense region of the monomer band. However, below 3550 cm^{-1} the stated CAVIAR uncertainties are smaller by a factor 5. The CAVIAR work shows large gaps and spectral structures which are not present in the new work. The SC differences are largest in the region where the monomer has strong lines and are in the range 0-10% of the strongest continuum features. The differences are outside the uncertainties stated for the CAVIAR work below 3550 cm^{-1} by up to a factor 10. The differences in this region appear to be a systematic error in the CAVIAR data since in Figure 7 the SC derived from independent air-broadened measurements agrees much better with the present results. Above 3550 cm^{-1} most data points are within the CAVIAR uncertainties. Regarding the uncertainties of the present work the differences are up to 10 times larger. In conclusion the present method for continuum determination yields substantial improvements. The differences between the present and the CAVIAR work reflect the impact of the different methods. The present method uses the entire spectrum, has thus no gaps and hence more information, but is very sensitive to the accurate representation of local lines. The CAVIAR method uses microwindows with smaller dependence on local lines. Furthermore, in case of the CAVIAR method the local line parameters are taken from spectroscopic databases and not from the spectra used to derive the continuum. Thus, errors from local lines do still exist although the sensitivity to local line errors is probably smaller than for the new method. Figure 17 shows that agreement of the high temperature data with CAVIAR is also reasonable. However, as already stated before, due to lack of sufficient measurements, the data quality of the present work's high temperature data is bad and the CAVIAR data are expected to be of much better quality.

Figure 17 also shows that the MT_CKD3.2 continuum model (and its earlier versions – see [Paynter2009]) is significantly weaker (by almost a factor of 10 at 3600 cm^{-1}) than the observed spectra between around 3500 and 3750 cm^{-1} and misses the two marked peaks near 3620 and 3730 cm^{-1}. We interpret that as being due to the fact that the MT_CKD3.2 continuum model does not include the bound dimer spectrum.

From the temperature dependence on Figure 17 it can clearly be seen that the continuum consists of two parts. One part (at wavenumbers below about 3800 cm^{-1}) looks similar to the modelled dimer spectrum and has a stronger temperature dependence. In Figure 5D in [Ptashnik2011] it can be seen that the ratio of SC(293 K) and SC(351 K) is about 2.7 at the pronounced dimer bands and about 2.0 away

from the bands. The temperature dependence of the in-band SC is investigated in detail in [Ptashnik2019].

Dimer band shape and dimerization constants

In the present work the dimer rovibrational band shape was modelled taking into account the expected band structure and type based on results of high resolution spectroscopy mostly in molecular beams. This allowed fitting of the SC resulting in tentative experimental dimer spectra which differ significantly from the prediction used in [Ptashnik2019]. In their work they fitted continua at different temperatures to a sum of modelled dimer bands and a quasi-bound dimer contribution calculated with a Voigt FWHM of 20 cm^{-1}. Residuals were up to 20% between 3550 and 3650 cm^{-1} and 45% around 3780 cm^{-1}, the modelled values are systematically too high above 3850 cm^{-1} (see Figure 5, ν_3, 296 K in [Ptashnik2019]). The fitted constants were K_{Db}=0.020(6) atm^{-1} and K_{Dq}=0.071(26) atm^{-1}. In the present work the corresponding values are 0.026(2) atm^{-1} and 0.044(5) atm^{-1}. While the K_{Db} values are similar the K_{Dq} value is smaller by 0.03 atm^{-1}. The residuals in the present work are of similar size around 3600 cm^{-1} but the agreement of the structure of the two peaks is better. Furthermore, the residuals around 3780 cm^{-1} are significantly smaller and the residuals above 3850 cm^{-1} are smaller, too.

Non-Lorentzian line wings as third SC component

As stated above [Serov2017] postulates that line wings of the monomer band that differ from the Voigt profile are a third component of the SC needed to resolve the discrepancy of the too large observed quasi-bound dimer spectrum when compared to the prediction from the equilibrium constant for the quasi-bound dimer. A multiplicative correction function for the Voigt profile, similar to the MT_CKD approach (see above), was defined. The parameter $\Delta\nu_{wing}$ was fixed to 11 cm^{-1} which leads to pronounced structures in the continuum (see Figure 2b in [Serov2017]). This had been based on the structures observed in the CAVIAR data which may result from limitations in the measurements or analysis since the SC in the present work looks significantly smoother (Figure 17) and has been validated by quality checks (see e.g. Figure 9). The structures observed in the CAVIAR data may be linked to the structure of the monomer spectrum itself, through the analysis process which uses troughs in the spectrum in combination with possibly erroneous local line parameters. Serov even uses the “spectral heterogeneity” to prove the non-Voigt line wing contribution to the continuum: that paper states that “The monomolecular nature of the excess continuum is also indirectly confirmed by its spectral heterogeneity. The dimeric absorption (a tremendous number of collisionally-broadened lines, which are more or less uniformly spread over the range) is very smooth. The spectrum of free-pairs is even

smoother due to the very short collision time causing the absorption. Therefore, the heterogeneity of the spectrum is the evidence that it belongs to the monomer line wings. A similar non-monotonicity of the water continuum, which is comparable with its measurement error in each separate transparency window, can be found in all wideband studies". The present work certainly does not support these statements. This does not rule out the line wing contribution but $\Delta\nu_{wing}$ must be substantially larger. However, the argument that the continuum structure proves the existence of a structured line wing contribution is not valid. Recently, [Odintsova2019] reported about the far-infrared pure rotation SC and found strong structure between 100 and 300 cm^{-1} which was tentatively attributed to local line problems and not to a structured SC.

As shown above, the results of the present work indicate the presence of a middle wing super-Lorentzian contribution. However, there was no high resolution structure found in contrast to Serov's results. The magnitude of the middle wing super-Lorentzian contribution suggests similarities with the FC which also does not show high resolution structure.

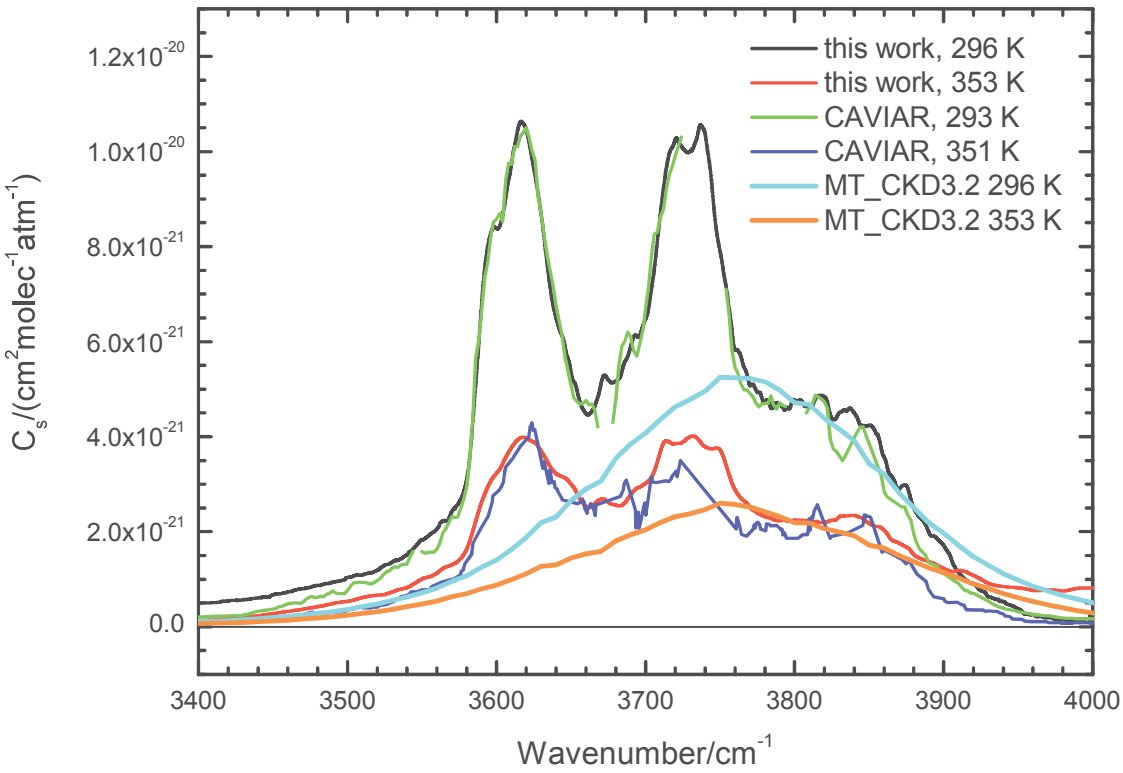

Figure 17. Comparison between different SCs and the dimer spectrum around 296 K. Experimental data at ca. 350 K are also shown. The base term [Paynter2009] was added to the SC from the current work in order to make it comparable to the other work. The wing correction applied for the FC (see below) could be neglected. CAVIAR data have been downloaded from http://www.met.reading.ac.uk/caviar/home/data.php.

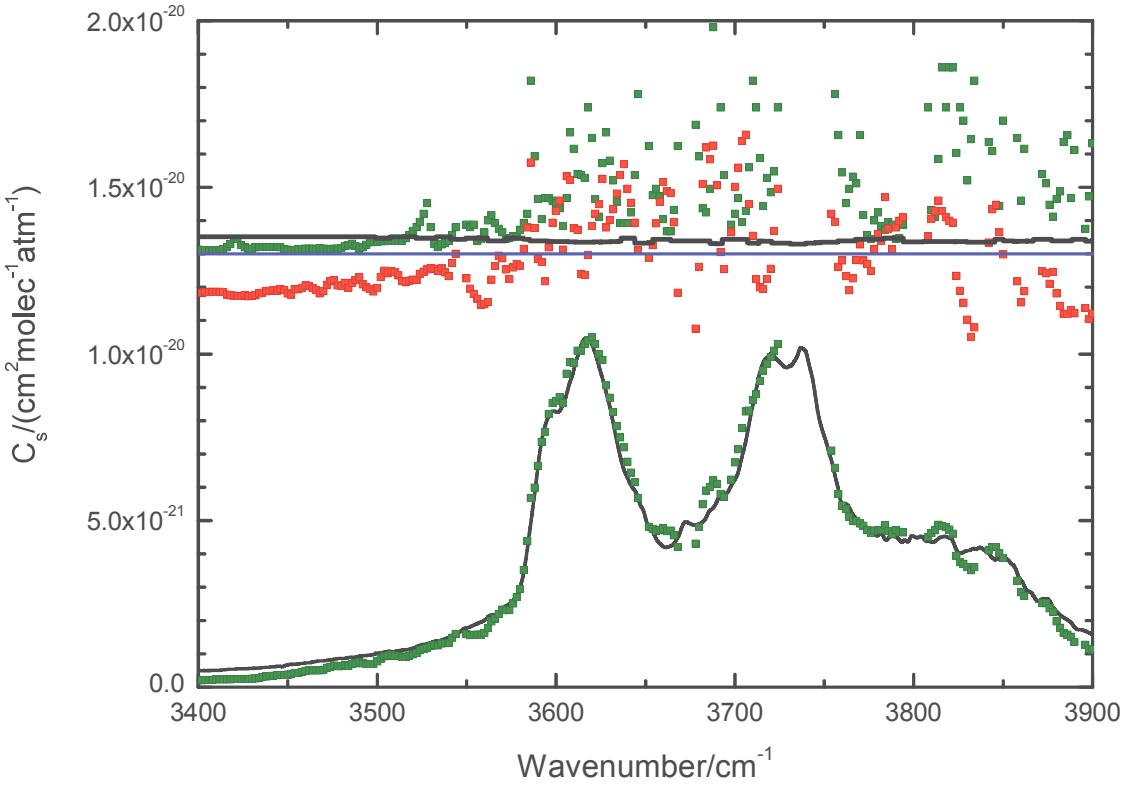

Figure 18. Comparison of CAVIAR and this work. Lower traces: black: SC this work, green: SC CAVIAR, upper traces multiplied by 4 and offset by 1.3×10^{-20} $cm^2molec^{-1}atm^{-1}$: black: uncertainty this work, green: uncertainty CAVIAR, red: CAVIAR – this work. CAVIAR data have been downloaded from http://www.met.reading.ac.uk/caviar/home/data.php.

5.2 Foreign-continuum

The FC for 296 K is compared to MT_CKD3.2 and the [Paynter2009] work in Figure 19. The base term had to be added to the FC of this work for intercomparison. It should be noted that the base term was introduced in the MT_CKD continuum model to ensure a smooth continuum [Mlawer2012]. For each line the intensity of the Lorentzian profile at 25 cm^{-1} away from the line center is taken to be part of the continuum for the whole spectral range ±25 cm^{-1} from the line center. The base term is the sum of all these "plinths". Furthermore, the sum of all line contributions >25 cm^{-1} and >100 cm^{-1} from line centers were calculated. Recall that the multispectrum fit cuts line profiles 100 cm^{-1} from line centers. In order to compare the original FC to Paynter and MT_CKD the >25 cm^{-1} contribution has to be added and the >100 cm^{-1} contribution has to be subtracted. This is equivalent to adding the missing contributions 25-100 cm^{-1}. The Paynter continuum is very noisy but on average shows good agreement with the present work. The MT_CKD3.2 FC is on average ca. 40% larger and has a significantly different shape, not showing P, Q and R-branch structure in contrast to the FC from the present work and the monomer band (see Figure 20). The black curve on Figure 19 is the FC without any local Voigt lines contribution.. We call this "physical continuum" because it contains only contributions not covered by the untruncated line model. In Figure 20 the smoothed monomer band, the MT_CKD3.2 continuum model and the red curve from Figure 19 are shown. While the MT_CKD3.2 continuum model and the FC from the present work have the same width, it is notable that they are narrower than the monomer band. The physical continuum from Figure 19 is even narrower. It was assured that the selection of the smoothing parameter has no significant influence on the apparent width of the monomer band. The mathematics causing the MT_CKD continuum model to be narrower than the monomer band can be found in [Mlawer2012] who introduced a lower state energy dependent weighting (see Eq. 3.3 therein) which decreases the weight in the wings of P- and R-branch, where transitions with high lower state energy dominate.

Concerning the physical nature of the FC there may be a link to the paper of [Tran2017] where HCl Argon broadening was measured and theoretically investigated. rCMDS (requantized Classical Molecular Dynamics Simulations) calculations were carried out in order to theoretically predict the line shape. rCMDS is based on purely classical trajectory calculations followed by re-establishing the quantized states. For details the reader is referred to [Tran2017] and references therein. The ratios of absorption cross sections in the troughs and the Lorentz values (fitted from the measurement) are similar to the ratios of calculated rCMDS absorption cross sections to Lorentz values fitted to rCMDS absorption cross sections. It should be mentioned that the Lorentzian widths deduced from the measurement and those obtained from rCMDS calculations show significant differences (see Figure 3 in [Tran2017]). So rCMDS appears to be good to calculate deviations from ideal behavior but not the lineshape in an absolute

manner. The dipole auto-correlation function was fitted to an expression which in the spectral domain was approximated by the sum of three Lorentzians. This sum can explain the super-Lorentzian behavior close to band center but not the sub-Lorentzian behavior for the band wings: [Tran2017] state that "the observed non-Lorentzian absorption results from two competitive mechanisms: (i) the behavior of the dipole autocorrelation at short times (related with collisions that are ongoing or start at t = 0) which induces super-Lorentzian effects; (ii) line-mixing (i.e., transfers of populations among the rotational levels) that reduces the absorption in the band wings and high *J* line regions and induces sub-Lorentzian effects." It is interesting to see that the FC has some similarity to the HCl/Ar spectra where intensity is transferred from the band wings to the band center. That the FC is narrower than the monomer band could also indicate an intensity transfer from the band wings to the center. Furthermore, a sub-Lorentzian behavior in the in-between band region also exists for the H_2O FC (see [Wagner2020]).

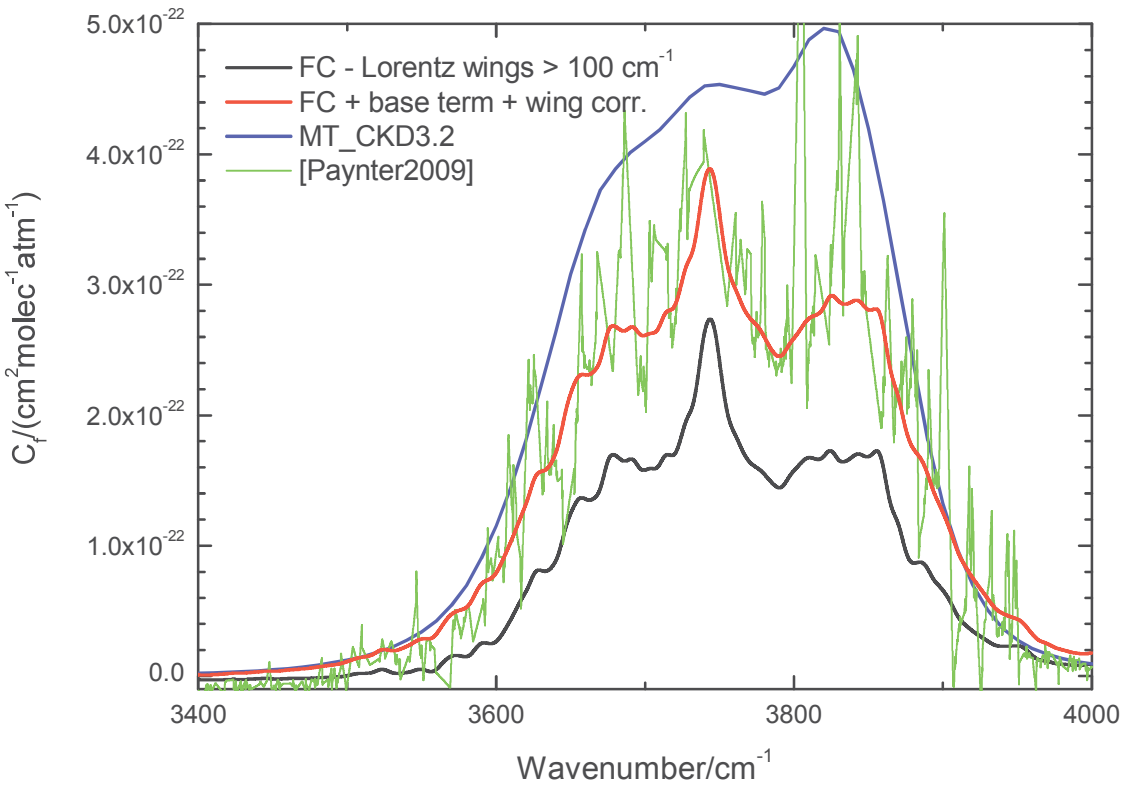

Figure 19. Comparison of FC. Wing correction refers to adding line contributions >25 cm^{-1} from line center and subtracting those >100 cm^{-1}. FC is obtained from the baseline fits of the present work. The black curve is the FC without any local lines Voigt contribution.

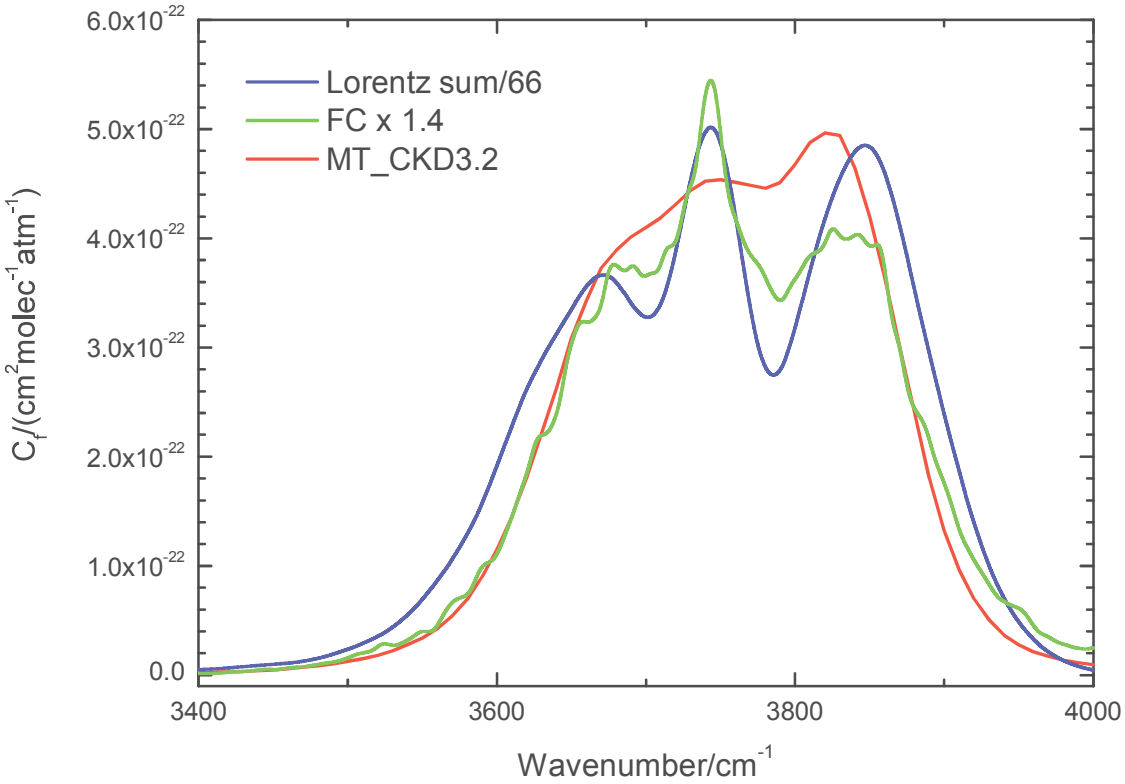

Figure 20. Comparison of MT_CKD3.2 FC with scaled smoothed Lorentz sum (smoothing kernel FWHM = 5 cm^{-1}, Lorentz HWHM = 0.5 cm^{-1}, parameters selected to show the low-resolution band shape) and scaled FC from present work. Scaling was introduced to have similar amplitude for better comparison.

6. Conclusion

A new method to derive the in-band SC and FC was developed. The method uses the same spectra to derive local line parameters and continua. It is essential to fit the local lines down to approximately the noise level to ensure that the fitted baseline only contains continuum information. The Hartmann-Tran profile in combination with Rosenkranz line mixing was required for accurate local line fitting. The method allowed the determination of the in-band SC for H_2O at 296 K in the 3 µm region without gaps and high spectral resolution of 2.4 cm^{-1}. Even in microwindows which were almost opaque, baseline and

thus continuum information was still available. In the case of the FC at 296 K there are also no gaps and the resolution was 7-16 cm^{-1}. The uncertainty in the FC was larger due to the high pressures and thus more congested spectra. Furthermore, the SC is also visible in the air-broadened spectra and thus SC errors are propagated into the FC. The new method for determining the continuum has led to considerably improved information content for SC and FC. Quality checks were used to validate the fitted continua. First, the SC was fitted from air-broadened measurements only and found to be in excellent agreement when compared with the SC from the self-broadened measurements. Second, residuals calculated from the original spectra and spectra modelled using local line parameters together with the continua are almost noise. SC and FC were also determined for 353 K, both from air-broadened measurements, but with less quality than the 296 K results due to the limited set of measurements.

Although the new self-continuum agrees well with the CAVIAR results between 3600 and 3800 cm^{-1} there are differences which exceed the uncertainties at higher and lower wavenumber. A significant advantage of the new self-continuum is that it is much smoother, has no gaps and is obtained with a high resolution of 2.4 cm^{-1}. The differences between the present and the CAVIAR work reflect the impact of the different methods. The new method uses the entire spectrum, has thus no gaps hence more information, but is very sensitive to the accurate representation of local lines. The CAVIAR method used microwindows with small dependence on local lines. Furthermore, the local line parameters are taken from spectroscopic databases and not from the spectra used to derive the continuum. Thus, errors from local lines do still exist although the sensitivity to local line errors is probably smaller than for the new method. The MT_CKD3.2 SC shows no bound dimer bands and differs significantly from both experimental SC datasets.

The self-continuum was fitted as sum of modeled bound and quasi-bound dimer spectra. From rotational constants the bound dimer parallel and perpendicular band shapes of the near prolate symmetric top molecule were calculated. Among the three strong dimer fundamentals in the 3 µm region, those linked to the H-O stretching vibration of the donor molecule, ν_1 and ν_3, have both parallel and perpendicular components while the asymmetric H-O stretch of the acceptor molecule, ν_9, is of purely perpendicular type. The quasi–bound dimer band shape was calculated from the spectroscopic database of the H_2O monomer for two cases with Voigt FWHM 20 cm^{-1} and 40 cm^{-1} for all lines. For the bound dimer fundamental wavenumbers, relative band intensities and partitioning of parallel and perpendicular band type were fitted, while the integral of the band intensities of the four fundamentals was fixed to published experimental/theoretical data. Dimerization constants for bound and quasi-bound dimers

were also fitted. The new approach allows modelling the observed continuum with unprecedented quality. Fit results for the H_2O dimer band centers and intensities were in reasonable agreement with experimental/theoretical literature data. In order to obtain physically meaningful results the band center of ν_9 as well as the parallel band contribution of ν_1 had to be fixed. A dimerization constant for the bound dimer of K_{Db}=0.026(2) atm^{-1} and the quasi-bound dimer of K_{Dq}=0.044(5) atm^{-1} was fitted. The sum, the total dimerization constant, was found to be too large by 0.018 atm^{-1} when compared to literature values. The excess was tentatively attributed to middle line wing super-Lorentzian contributions of the H_2O monomer lines, resulting in a dimerization constant for the quasi-bound dimer of K_{Dq}'=0.026 atm^{-1}.

We suggest applying the fit procedure introduced in the present work also to the continuum data at temperatures other than 296 K, published in [Ptashnik2019]. The temperature dependence may provide more insights on the nature of contributions to the in-band SC. The investigation of other strong fundamental regions, like the bands around 1600 cm^{-1}, applying the new method would furthermore improve the understanding on the continuum.

The FC at 296 K agrees with the Paynter results but is much less noisy and has no gaps in spectral coverage. It is on average about 40% smaller than the MT_CKD3.2 FC model and shows a very different shape. It has a pronounced P, Q, and R branch structure barely visible in the more noisy Paynter results. Both, the FC from present work and the MT_CKD FC model appear narrower than the monomer band which may be of interest regarding the physical nature of the FC. Certainly, the new method has larger benefits for FC than SC determination since the impact of local lines is larger for the FC due to the higher pressure needed (resulting in broader lines) since the FC is much weaker than the SC.

The method presented here will be improved by fitting the continuum and line parameters simultaneously in the multispectrum fitting approach. Certainly, dedicated measurements with optimized pressure and temperature steps and high baseline quality will help to provide excellent continuum data with the new method, which can be extended to derive the continuum in other water vapor bands.

Acknowledgements

The measurement of the spectra and the previous line parameter analysis have been performed within the framework of the DFG projects under contract numbers BI 834/5-1 and BI 834/5-2. KPS

acknowledges support from the UK Natural Environment Research Council (grant number NE/R009848/1). The authors thank David Paynter for providing the data in Figure 19 in digital form and for answering queries, and the reviewers of the original submission this paper for triggering several essential improvements.

Appendix A. Supplementary material

Supplementary data associated with this article can be found in the online version at http://dx.doi.org/.... FC and SC at 296 K together with uncertainties are given in ASCII files FC_H2O_3mu.txt and SC_H2O_3mu.txt, first column wavenumber, second column continuum coefficient in $cm^2molec^{-1}atm^{-1}$, third column uncertainty in $cm^2molec^{-1}atm^{-1}$.

References

[Birk2016] Birk M, Wagner G. Voigt profile introduces optical depth dependent systematic errors – Detected in high resolution laboratory spectra of water. J Quant Spectrosc Radiat Transfer 2016;170:159-168. http://doi.org/10.1016/j.jqsrt.2015.11.008.

[Burch1982] Burch DE. Continuum absorption by H_2O. AFGL-TR 1982;81:0300. http://dx.doi.org/10.1117/12.931899.

[Burch1984] Burch DE, Alt RL. Continuum absorption by H_2O in the 700-1200 cm^{-1} and 2400-2800 cm^{-1} windows. AFGL-TR 1982;84:0128.

[Burch1985] Burch, DE, Absorption by H_2O in narrow windows between 3000 – 4200 cm^{-1}, AFGL-TR 1985;85–0036. Air Force Geophys. Lab., Hanscom AFB, Mass.

[Campargue2016] Campargue A, Kassi S, Mondelain D, Vasilchenko S, Romanini D. Accurate laboratory determination of the near-infrared water vapor selfcontinuum: A test of the MT_CKD model. J Geophys Res Atmos 2016;121:13,180–13,203. http://doi.org/10.1002/2016JD025531.

[Ceponkus2008] Ceponkus J, Uvdal P, Nelander B. Far-Infrared Band Strengths in the Water Dimer: Experiments and Calculations. J. Phys. Chem. A 2008;112:3921-3926. http://doi.org/10.1021/jp711178w.

[Clough1989] Clough SA, Kneizys FX, Davies RW. Line Shape and the Water Vapour Continuum. Atm Res 1989;23:229-41. http://dx.doi.org/10.1016/0169-8095(89)90020-3.

[Cole2015] Cole WTS, Fellers RS, Viant MR, Leforestier C, Saykally RJ. Far-infrared VRT spectroscopy of the water dimer: Characterization of the 20 µm outof-plane librational vibration. J. Chem. Phys 2015;143:154306. http://dx.doi.org/10.1063/1.4933116.

[Cormier2005] Cormier JG, Hodges JT, Drummond JR. Infrared water vapour continuum absorption at atmospheric temperatures, J Chem Phys 2005;122:114309. http://doi.org/10.1063/1.1862623.

[Epifanov1997] Epifanov SYu, Vigasin AA. Subdivision of phase space for anisotropically interacting water molecules. Mol. Phys. 1997;90(1):101-106.

[Gordon2017] Gordon IE, Rothman LS, Hill Chr, Kochanov R, Yan T, Bernath PF, Birk M, Boudon V, Camparque A, Chance K, Drouin BJ, Flaud J-M, Gamache RR, Hodges JT, Jacquemart D, Perevalov VI, Perrin A, Shine KP, Smith MAH, Tennyson J, Toon GC, Tran H, Tyuterev VIG, Barbe A, Csaszar A, Devi V, Loos J, Wagner G, Wilzewski J, et al. The HITRAN2016 Molecular Spectroscopic Database, J Quant Spectrosc Radiat Transfer 2017;203:3-69. http://doi.org/10.1016/j.jqsrt.2017.06.038.

[Herzberg1945] Herzberg G. Molecular spectra nad molecular structure, II. Infrared and Raman spectra of polyatomic molecules. Van Nostrand, New York.

[Huang1988] Huang ZS, Miller RE. Sub-Doppler resolution infrared spectroscopy of water dimer. J. Chem. Phys. 1988;88:8008. http://doi.org/10.1063/1.454258.

[Huang1989] Huang ZS, Miller RE. High-resolution near-infrared spectroscopy of water dimer. J. Chem. Phys. 1989;91:6613. http://doi.org/10.1063/1.457380.

[Kapitanov2018] Kapitanov VA, Osipov KY, Ptashnik IV. Photoacoustic measurements of the water vapor continuum absorption in the 1.6 µm window, Optika Atmosfery i Okeana 2018;31:995-1000, in Russian

[Kjaergaard2008] Kjaergaard HG, Garden AL, Chaban GM, Gerber RB, Matthews DA, Stanton JF. Calculation of Vibrational Transition Frequencies and Intensities in Water Dimer: Comparison of Different Vibrational Approaches. J Phys Chem A 2008;112:4324-4335. http://doi.org/10.1021/jp710066f.

[]Koshelev2018] Koshelev MA, Leonov II, Serov EA, Chernova AI, Balashov AA, Bubnov GM, Aleksandr FA, Shkaev AP, Parshin VV, Krupnov AF, Tretyakov MYu. New Frontiers in Modern Resonator Spectroscopy. IEEE TRANSACTIONS ON TERAHERTZ SCIENCE AND TECHNOLOGY 2018;8:773-783. http://doi.org/10.1109/TTHZ.2018.2875450.

[Kuyanov-Prozument2010] Kuyanov-Prozument K, Choi MY, Vilesov AF. Spectrum and infrared intensities of OH-stretching bands of water dimers. J Chem Phys 2010;132:014304. http://doi.org/10.1063/1.3276459.

[Kuyanov-Prozument2010] Kuyanov-Prozument K, Choi MY, Vilesov AF. Spectrum and infrared intensities of OHstretching bands of water dimers. J Chem Phys 2010;132:014304.

[Lechevallier2018] Lechevallier L, Vasilchenko S, Grilli R, Mondelain D, Romanini D, Campargue A. The water vapour self-continuum absorption in the infrared atmospheric windows: new laser measurements near 3.3 and 2.0 µm. Atmos Meas Tech 2018;11:2159–2171. http://doi.org/10.5194/amt-11-2159-2018.

[Loos2017] Loos J, Birk M, Wagner G. Measurement of positions, intensities and self-broadening line shape parameters of H_2O lines in the spectral ranges 1850-2280 cm^{-1} and 2390-4000 cm^{-1}. J Quant Spectrosc Radiat Transfer 2017;203:119-32. http://doi.org/10.1016/j.jqsrt.2017.02.013.

[Loos2017a] Loos J, Birk M, Wagner G. Measurement of air-broadening line shape parameters and temperature dependence parameters of H_2O lines in the spectral ranges 1850-2280 cm^{-1} and 2390-4000 cm^{-1}. J Quant Spectrosc Radiat Transfer 2017;203:103-18. http://doi.org/10.1016/j.jqsrt.2017.03.033.

[Ma2008] Ma Q, Tipping RH, Leforestier C, Temperature dependences of mechanisms responsible for the water-vapour continuum absorption. I. Far wings of allowed lines, J Chem Phys 2008;128:124313. http://doi.org/10.1063/1.2839604.

[Mlawer2012] Mlawer EJ, Payne VH, Moncet J-L, Delamere JS, Alvarado MJ, Tobin DC. Development and recent evaluation of the MT_CKD model of continuum absorption. Phil Trans R Soc A 2012;370:2520-56. http://dx.doi.org/10.1098/rsta.2011.0295.

[Mlawer2019] Mlawer EJ, Turner DD, Paine SN, Palchetti L, Bianchini G, Payne VH, et al. Analysis of water vapor absorption in the far-infrared and submillimeter regions using surface radiometric measurements from extremely dry locations. J Geophys Res: Atmospheres 2019;124:8134–8160. https://doi.org/10.1029/2018JD029508.

[Mondelain2015] Mondelain D, Vasilchenko S, Cermak P, Kassi S, Campargue A. The self- and foreign-absorption continua of water vapor by cavity ring-down spectroscopy near 2.35 µm. Phys Chem Chem Phys 2015;17:17762. http://doi.org/10.1039/C5CP01238D.

[Mondelain2020] Mondelain D, Vasilchenko S, Kassi S, Campargue A. The water vapor foreign-continuum in the 1.6 µm window by CRDS at room temperature. J Quant Spectrosc Radiat Transfer 2020;246:106923. https://doi.org/10.1016/j.jqsrt.2020.106923.

[Mukhopadhyay2015] Mukhopadhyay A, Cole WTS, Saykally RJ. The water dimer I: Experimental characterization. Chem Phys Let 2015;633:13–26. http://doi.org/10.1016/j.cplett.2015.04.016.

[Newman2012] Newman et al., Airborne and satellite remote sensing of the mid-infrared water vapour continuum, Phil Trans R Soc A 2012;370:2611–2636. http://dx.doi.org/10.1098/rsta.2011.0223.

[Odintsova2014] Odintsova TA, Tretyakov MYu, Krupnov AF, Leforestier C. The water dimer millimeter-wave spectrum at ambient conditions: A simple model for practical applications. J Quant Spectrosc Radiat Transfer 2014;140:75–80. http://dx.doi.org/10.1016/j.jqsrt.2014.02.016

[Odintsova2019] Odintsova TA, Tretyakov MYu, Zibarova AO, Pirali O, Roy P, Campargue A. Far-infrared self-continuum absorption of $H_2{}^{16}O$ and $H_2{}^{18}O$ (15-500 cm^{-1}). J Quant Spectrosc Radiat Transfer 2019;227:190-200. http://dx.doi.org/10.1016/j.jqsrt.2019.02.012.

[Paynter2009] Paynter DJ, Ptashnik IV, Shine KP, Smith KM, McPheat R, and Williams RG. Laboratory measurements of the water vapour continuum in the 1200–8000 cm^{-1} region between 293 K and 351 K, J Geophys Res 2009;114:D21301. http://dx.doi.org/10.1029/2008JD011355.

[Paynter2011] Paynter DJ, Ramaswamy V. An assessment of recent water vapor continuum measurements upon longwave and shortwave radiative transfer. J Geophys Res 2019;116:D20302. http://dx.doi.org/10.1029/2010JD015505.

[Ptashnik2004] Ptashnik IV, Smith KM, Shine KP, Newnham DA. Laboratory measurements of water vapour continuum absorption in spectral region 5000-5600 cm^{-1}: Evidence for water dimers Quart J Roy Met Soc 2004;130:2391-2408. http://doi.org/10.1256/qj.03.178.

[Ptashnik2011] Ptashnik IV, Shine KP, Vigasin AA. Water vapour self-continuum and water dimers: 1. Analysis of recent work. J Quant Spectrosc Radiat Transfer 2011;112:1286–1303. http://doi.org/10.1016/j.jqsrt.2011.01.012.

[Ptashnik2012] Ptashnik IV, McPheat RA, Shine KP, Smith KM, Williams RG. Water vapour foreign-continuum absorption in near-infrared windows from laboratory measurements. Phil Trans R Soc A 2012;370:2557–2577. http://dx.doi.org/10.1098/rsta.2011.0218.

[Ptashnik2019] Ptashnik IV, Klimeshina TE, Solodov AA, Vigasin AA. Spectral composition of the water vapour self-continuum absorption within 2.7 and 6.25 µm bands. J Quant Spectrosc Radiat Transfer 2019;228:97–105. http://doi.org/10.1016/j.jqsrt.2019.02.024.

[Richard2017] Richard L, Vasilchenko S, Mondelain D, Ventrillard I, Romanini D, Campargue A. Water vapor self-continuum absorption measurements in the 4.0 and 2.1 µm transparency windows. J Quant Spectrosc Radiat Transfer 2017;201:171–179. http://dx.doi.org/10.1016/j.jqsrt.2017.06.037.

[Scribano2007] Scribano Y, Leforestier C. Contribution of water dimer absorption to the millimeter and far infrared atmospheric water continuum. J. Chem. Phys. 2007;126:234301. http://doi.org/10.1063/1.2746038.

[Serov2014] Serov EA, Koshelev MA, Odintsova TA, Parshin VV, Tretyakov MYu. Rotationally resolved water dimer spectra in atmospheric air and pure water vapour in the 188–258 GHz range. Phys Chem Chem Phys 2014;16:26221. http://doi.org/10.1039/c4cp03252g.

[Serov2017] Serov EA, Odintsova TA, Tretyakov MYu, Semenov VE. On the origin of the water vapour continuum absorption within rotational and fundamental vibrational bands, J Quant Spectrosc Radiat Transfer 2017;193:1–12, http://doi.org/10.1016/j.jqsrt.2017.02.011.

[Shine2012] Shine KP, Ptashnik IV, Rädel G. The Water Vapour Continuum: Brief History and Recent Developments. Surv Geophys 2012;33:535-55. http://dx.doi.org/10.1007/s10712-011-9170-y.

[Shine2016] Shine KP, Campargue A, Mondelain D, McPheat RA, Ptashnik IV, Weidmann D. The water vapour continuum in near-infrared windows – Current understanding and prospects for its inclusion in spectroscopic databases. J Mol Spectrosc 2016;327:193–208. http://dx.doi.org/10.1016/j.jms.2016.04.011.

[Tipping1995] Tipping RH, Ma Q. Theory of water-vapour continuum and validations. Atmos Res 1995;36:69-94. http://dx.doi.org/10.1016/0169-8095(94)00028-C.

[Tran2013] Tran H, Ngo NH, Hartmann J-M. Efficient computation of some speed-dependent isolated line profiles. J Quant Spectrosc Radiat Transfer 2013;129:199-203. http://doi.org/10.1016/j.jqsrt.2013.06.015.

[Tran2014] Tran H, Ngo NH, Hartmann J-M. Erratum to “Efficient computation of some speed-dependent isolated line profiles”. J Quant Spectrosc Radiat Transfer 2014;134:104. http://doi.org/10.1016/j.jqsrt.2013.10.015.

[Tran2017].Tran H, Li G, Ebert V, Hartmann J-M. Super- and sub-Lorentzian effects in the Ar-broadened line wings of HCl gas. J Chem Phys 2017;146:194305. http://doi.org/10.1063/1.4983397.

[Tretyakov2013] Tretyakov MYu Serov EA, Koshelev MA, Parshin VV, Krupnov AF. Water Dimer Rotationally Resolved Millimeter-Wave Spectrum Observation at Room Temperature. Phys Rev Let 2013;110:093001. http://doi.org/10.1103/PhysRevLett.110.093001.

[Tso1998] Tso HCW, Geldart DJW, Chýlek P. Anharmonicity and cross section for absorption of radiation by water dimer. J Chem Phys 1998;108:5319. https://doi.org/10.1063/1.475967

[Vasilchenko2019] Vasilchenko S, Campargue A, Kassi S, Mondelain D. The water vapour self- and foreign-continua in the 1.6 µm and 2.3 µm windows by CRDS at room temperature, J Quant Spectrosc Radiat Transfer 2019;227:230–238. http://doi.org/10.1016/j.jqsrt.2019.02.016.

[Wagner2020] Wagner G, Birk M, Tretyakov MYu. What we learn by subtracting Lorentzian line wings beyond 25 cm^{-1} from the MT_CKD H_2O continua. , J Quant Spectrosc Radiat Transfer, this issue.

Declaration of interests

 The authors declare that they have no known competing financial interests or personal relationships that could have appeared to influence the work reported in this paper.

☐The authors declare the following financial interests/personal relationships which may be considered as potential competing interests:

Author statement

Manfred Birk: Conceptualization, Methodology, Software, Formal analysis, Investigation, Writing - Original Draft, Writing - Review & Editing, Visualization, Supervision, Project administration, Funding acquisition

Georg Wagner: Conceptualization, Methodology, Software, Formal analysis, Investigation, Writing - Original Draft, Writing - Review & Editing, Visualization

J. Loos: Software, Investigation, Formal analysis, Writing - Original Draft

Keith P. Shine: Writing - Original Draft, Writing - Review & Editing